CHAPTER 2
Applied Linear-Systems Theory

Ian A. Cunningham
John P. Robarts Research Institute, and London Health Sciences Centre

CONTENTS

2.1 Introduction

A wide variety of both digital and nondigital medical-imaging systems are now in clinical use and many new system designs are under development. These are all complex systems, with multiple physical processes involved in the conversion of an input signal (e.g., x rays) to the final output image viewed by the interpreting physician. For every system, a high-quality image is obtained only when all processes are properly designed so as to ensure accurate transfer of the image signal and noise from input to output.

An important aspect of imaging science is to understand the fundamental physics and engineering principles of these processes, and to predict how they influence final image quality. For instance, it has been known since the work of Rose [1–4], Shaw [5], and others that the image signal-to-noise ratio (SNR) is ultimately limited by the number of quanta used to create the image. This is illustrated in Figure 2.1, showing the improvement in image quality as the number of x-ray quanta used to produce images of a skull phantom is increased from 45 to 6720 quanta/mm^2. Negligible image noise was added by the imaging system.

The view that an imaging system must faithfully *transfer* the input image signal to the output suggested the use of foundations laid out by scientists and engineers studying communications theory, and in particular, use of the Fourier-
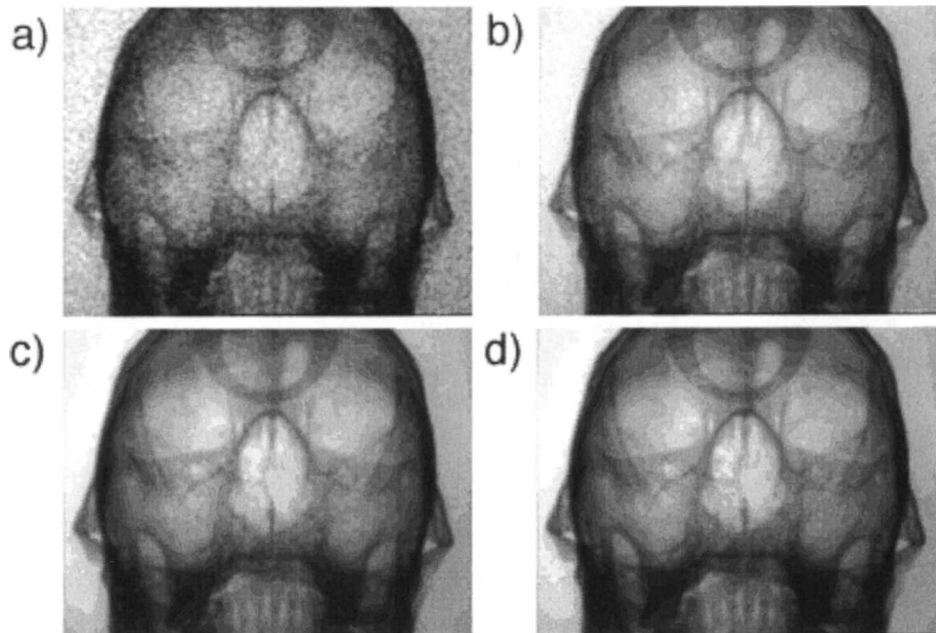
Figure 2.1: Image quality is dependent on the number of quanta used to create an image as illustrated in this example. The average detector x-ray exposure per image is approximately: a) 0.16 μR, b) 1.6 μR, c) 16 μR, and d) 24 μR.

Table 2.1: Summary of incident detector exposure and number of quanta per mm^2 used to create the images shown in Figure 2.1

	Detector Exposure	Quanta per mm^2
a)	$0.16\,\mu R$	45
b)	$1.6\,\mu R$	450
c)	$16\,\mu R$	4500
d)	$24\,\mu R$	6720

transform linear-systems approach [6]. Linear-systems theory was initially applied in the imaging sciences by Rossmann and co-workers [7, 8], including use of the modulation-transfer function (MTF) and related concepts. General works have subsequently been published by Dainty and Shaw [5], Gaskill [9], Papoulis [10], Doi, Rossmann and Haus [11], Metz and Doi [12], and others. Possibly the most extensive use of linear-systems theory in the medical-imaging field is the comprehensive text by Barrett and Swindell [13] who use this approach to describe fundamental principles and characteristics of many imaging systems in radiography, computed tomography (CT), nuclear medicine, ultrasound, and other areas.

In this chapter, principles of linear-systems theory as it pertains to the analysis of medical-imaging systems are described. The linear-systems approach is used to describe both signal and noise transfer, for both digital and nondigital systems. The link is made to metrics of image and system quality including the modulation-transfer function (MTF), noise-equivalent number of quanta (NEQ), quantum sinks, and detective quantum efficiency (DQE). For background reading, see Bracewell [14] for an excellent description of the Fourier transform, and Brigham [15] for a description of the discrete Fourier transform. General references for stochastic processes are Bendat and Piersol [16] and Papoulis [17]. The noise-power spectrum is described by Dainty and Shaw [5] and Blackman and Tukey [18].

2.2 Background concepts

2.2.1 Images and their units

The input to an x-ray imaging system is always a distribution of x-ray quanta. The output may be approximated as an analog image such as the optical density of a film transparency, or a digital image consisting of an array of digital values stored in computer memory. The term "image" may be used to represent each of these three types of quantities, giving rise to three different types of images: (1) an analog image, $d(r)$; (2) a digital image, d_n; and (3) a distribution of quanta forming a quantum image, $q(r)$. These particular names are the author's preference, but the distinctions are necessary as they have different units and physical meanings, and must therefore be treated differently mathematically.

Transfer theory provides a description of the relationships between these three quantities. In particular, it is used here to describe the relationship between an input quantum image (generally a distribution of x-ray quanta incident on a detector) and an output analog or digital image. In this section, these three types of images and their physical bases are described.

2.2.1.1 Analog image

The term *analog image* will be used to describe a spatially-varying sample function $d(r)$. It is expressed as a function of the continuous variable r representing position in an n-dimensional image. The units of $d(r)$ are arbitrary. Examples include the voltage from a video camera as a function of position along a trace, optical density in a radiographic film, or mean emitted intensity from a CRT monitor.

2.2.1.2 Digital image

A *digital image* generally consists of an n-dimensional array of discrete numerical values. For example, d_{n_x,n_y} represents image intensity at a particular pixel (picture element) in a two-dimensional image identified by the coordinate n_x, n_y. These values may be used as an index into a "look-up table" to produce the desired image brightness according to a specified display level and window. The values d_{n_x,n_y} are dimensionless, as are the digital values produced by an analog-to-digital converter (ADC).

2.2.1.3 Quantum image

A *quantum image* is a spatial distribution of quanta. For example, x rays transmitted through a patient and incident on an imaging detector form an x-ray quantum image. Each quantum has negligible spatial extent, and may be considered to be a point or impulse object represented as a single Dirac delta function $\delta(r - r_0)$ where r_0 is a vector describing the location of the quantum. Therefore, a quantum image may be represented as the sample function $q(r)$ consisting of the superposition of a large number of spatially-distributed δ functions.

There are two important reasons why manipulating quantum images is more complicated than manipulating analog or digital images. The first is that they must be interpreted as *distributions* in the mathematical sense, having dimension area^{-1} for a two-dimensional image. Some implications of this are described in more detail below. The second reason is that image quanta have fundamental statistical properties that cannot be ignored. It is therefore necessary to interpret $q(r)$ as a sample function of a random process. For instance, we describe the position of each quantum in an image using the random vector variable $\bar{r}$ which has the set of values $\{r_i\}$ and where each value describes the position of one quantum. The quantum image $q(r)$ is a particular realization of these random variables, and can be expressed as the sample distribution

$$q(r) = \sum_{i=1}^{N_q} \delta(r - r_i). \tag{2.1}$$

While it is not possible to know *precisely* where the x-ray quanta are in a particular distribution because of the uncertainty principle, $q(r)$ represents a particular *possible* distribution. That is, a sample image, where the quanta may be statistically correlated—or not—in some specified way. The expected value (i.e., an ensemble average of many such realizations, see Section 2.5.2) of $q(r)$ will be written as $E\{q(r)\}$, and describes the expected distribution of quanta per unit area at position r. If the image consists only of a Poisson distribution of quanta, $\tilde{r}$ is randomly distributed and uncorrelated over the image area, and $E\{q(r)\}$ is a constant independent of position.

Quantum images are generally two dimensional. However, it will be convenient, particularly for illustrations, to consider a one-dimensional quantum image consisting of a distribution of quanta along a line, $q(x)$, having dimension length^{-1}.

2.2.2 The Dirac δ function, sampling, and the sifting property

The Dirac δ function, or impulse function, is so important in the application of linear-systems theory, both for the representation of quantum images as described above and in the analysis of digital systems, that it is appropriate to describe its properties explicitly. The symbol $\delta(x - x_0)$ represents an impulse at position x_0 with the property that [14]

$$\delta(x - x_0) = \begin{cases} 0 & \text{for } x \neq x_0 \\ \text{undefined} & \text{for } x = x_0, \end{cases} \tag{2.2}$$

and with the constraint that

$$\int_{-\infty}^{\infty} \delta(x - x_0)\, dx = 1. \tag{2.3}$$

The δ function always has a dimension corresponding to the inverse of its argument (x^{-1} in this case). In addition, for any function $f(x)$ that is continuous at $x = x_0$,

$$\int_{a}^{b} f(x)\delta(x - x_0)\, dx = \begin{cases} f(x_0) & \text{if } a < x_0 < b \\ 0 & \text{otherwise}, \end{cases} \tag{2.4}$$

and from which comes the *sifting* property,

$$\int_{-\infty}^{\infty} f(x)\delta(x - x_0)\, dx = f(x_0) \int_{-\infty}^{\infty} \delta(x - x_0)\, dx = f(x_0) = f(x)|_{x=x_0}. \tag{2.5}$$

The sifting property provides a mechanism whereby the process of *sampling*, that is, evaluating a function at a specified position $x = x_0$, can be expressed in terms of the linear operation of multiplication with a δ function:

$$f(x)\delta(x - x_0) = f(x_0)\delta(x - x_0). \tag{2.6}$$

It is important to note that multiplication with the δ function does not result in the sample value alone—it results in a δ function *scaled* by the sample value $f(x_0)$. The sample value may be dimensionless, but the δ function is not.

The δ function is a *generalized* function in the mathematical sense as opposed to a "well-behaved" function. For this reason it is sometimes referred to as the δ symbol rather than the δ function. While it is tempting to manipulate the δ function as if it were well behaved, it is really defined only in terms of its properties, such as those given by Eqs. (2.2) to (2.5), and must be treated accordingly, and with great care.

In addition to the sifting property, other important properties of the δ function include [14]

$$\delta(ax) = \frac{1}{|a|}\delta(x), \tag{2.7}$$

$$\delta(-x) = \delta(x), \tag{2.8}$$

$$x\delta(x) = 0. \tag{2.9}$$

The Dirac δ function should not be confused with the Kronecker δ function, defined as

$$\delta_m = \begin{cases} 1 & \text{for } m = 0 \\ 0 & \text{for } m \neq 0, \end{cases} \tag{2.10}$$

often used in the description of discrete systems.

2.2.3 Generalized functions

While use of the δ function is often convenient, it must again be emphasized that it is a *generalized* function, and must be treated with care. The δ function was first used by physicists for the description of momentum impulses and point objects such as point charges. While the δ function is not a real function, it was often manipulated as if it were. With the subsequent development of generalized functions, it is known now that the δ function can often be manipulated as a real function but only evaluated within an integral as expressed by the sifting property in Eq. (2.5).

The class of generalized functions used here can be defined as the limit of a sequence of well-behaved functions. The one-dimensional δ function can be expressed in terms of many such limits, two being

$$\delta(x) = \lim_{\tau \to \infty} \frac{\sin(\pi \tau x)}{\pi x} = \lim_{\tau \to \infty} \tau \text{sinc}(\pi \tau x), \tag{2.11}$$

and

$$\delta(x) = \lim_{\tau \to \infty} \frac{\sin^2(\pi \tau x)}{\pi^2 \tau x^2} = \lim_{\tau \to \infty} \tau \text{sinc}^2(\pi \tau x). \tag{2.12}$$

Refer to Bracewell [14] or Gaskill [9] for a description of δ functions, distributions, and generalized functions in linear-systems theory.

2.2.4 Distribution theory

Images consisting of a distribution of quanta *must* be interpreted using distribution theory. A distribution can be measured only through the use of a *sampling function*, $\phi(x)$ which describes the measurement process. The sampling function is sometimes called an *aperture function* when used to describe the sensitivity profile of a detector. Do not confuse it with the sampling operation where a waveform is multiplied with a δ function (Section 2.2.2), or a sample function of a stochastic process (Section 2.5). For example, if a measure of the one-dimensional quantum image $q(x)$ is obtained with a detector of width a, producing a signal proportional to the number of interacting quanta, the result d may be expressed as the integral

$$d = k \int_{x_0-a/2}^{x_0+a/2} q(x)\,\mathrm{d}x = k \int_{-\infty}^{\infty} q(x) \prod\left(\frac{x-x_0}{a}\right) \mathrm{d}x, \qquad (2.13)$$

where the detector is centered at $x = x_0$ and k is a constant relating the number of interacting quanta to the detector output signal that might be a voltage, or an analog-to-digital converter (ADC) value (assuming ADC quantization errors can be ignored). In this example, the sampling function is $\phi(x) = \Pi(x/a)$ which is a rectangle of unity height and width a.

Note that while $q(x)$ is a generalized function, the expected value of $q(x)$, $E\{q(x)\}$, is a well-behaved function having the same units.

2.2.5 Transfer theory

One way of characterizing an imaging system is to describe the input-output relationships of parameters useful in the description of image signals and noise. For instance, Figure 2.2 shows input and output images, $q_{in}(r)$ and $q_{out}(r)$ respectively, of a hypothetical imaging system in which there has been a degradation of image contrast.

2.2.5.1 Signals: large-area contrast transfer

Contrast is a measure of the relative brightness difference between two locations in an image. Relative brightness is often a more important parameter than absolute brightness because the absolute brightness of a displayed image is often dependent on the display hardware (e.g., video monitor brightness setting or viewbox intensity), and may therefore have no particular significance in an absolute sense. The contrast between locations r_1 and r_2 of $q_{in}(r)$ in Figure 2.2 is C_{in}, defined as

$$C_{in} = \frac{E\{q_{in}(r_2)\} - E\{q_{in}(r_1)\}}{\frac{1}{2}[E\{q_{in}(r_2)\} + E\{q_{in}(r_1)\}]}. \qquad (2.14)$$

An alternative definition of contrast used by some omits the factor $1/2$ but is not used in this chapter. The corresponding contrast in the output image is C_{out} where

$$C_{out} = \frac{\mathrm{E}\{q_{out}(r_2)\} - \mathrm{E}\{q_{out}(r_1)\}}{\frac{1}{2}[\mathrm{E}\{q_{out}(r_2)\} + \mathrm{E}\{q_{out}(r_1)\}]}, \tag{2.15}$$

and the large-area contrast-transfer factor is therefore defined as the ratio

$$T_c = \frac{C_{out}}{C_{in}}. \tag{2.16}$$

The concepts of signal transfer are related to the spatial resolution of a system. This is illustrated in Figure 2.3 where the input-output relationship is shown for a system that transfers large-area (relative to the measurement area) contrast fairly well, but small-area contrast poorly. The result is an output image in which the contrast of fine details (small lesions and edges) is reduced, giving rise to an image that appears to be "blurred" by the system.

Transfer theory must therefore be tied somehow to concepts of both image-structure size and system spatial resolution. One way of doing this is to express
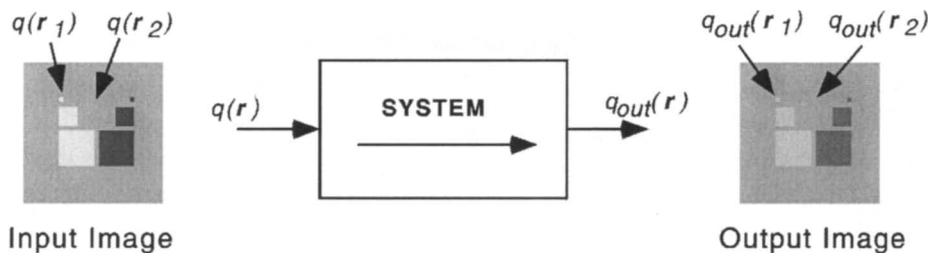
Figure 2.2: Transfer theory describes relationships between the input and output images of an imaging system. In this illustration of a deterministic system, an image is transferred accurately except for a degradation in contrast.
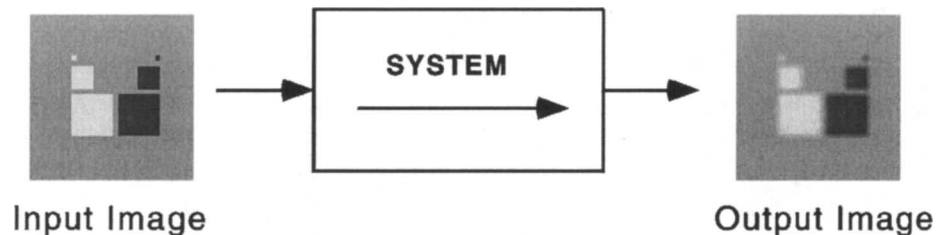
Figure 2.3: A system with poor spatial resolution transfers large-area contrast better than small-area contrast. As a result, the contrast of fine detail is reduced and the transferred image appears "blurred."

transfer relationships in the spatial-frequency domain and to make extensive use of the Fourier transform and related theorems. The uniqueness of the Fourier transform means that any problem can be solved equivalently in either the spatial (r) or the spatial-frequency (k) domains. It is often easier to find a solution in one domain than in the other, and so every imaging problem should be examined in both. In addition, important insight is often obtained when the solution to any problem is expressed in each domain. For instance, the harmful effect of signal and noise aliasing is easier to predict in the spatial-frequency domain, but it may be necessary to understand aliasing in the spatial domain to develop a physical intuition of the outcome. *The importance of being able to move fluently between the two domains cannot be overstated, and in the opinion of some, is one of the important distinguishing skills of an imaging scientist.*

2.2.5.2 Noise: variance transfer

Contrast transfer says nothing about the transfer of image noise as illustrated in Figure 2.4. Image noise is defined here as stochastic variations in image signals (see Section 2.5.2). For instance, an image of a uniform object might have a uniform intensity over a specified region of interest if not for these random variations. One way of describing noise is to calculate the variance in measurements of the image signal over a specific region of interest which has a uniform expected value. Noise variance is then given as [10]

$$\sigma_d^2 = \mathrm{E}\{|\Delta d|^2\}, \tag{2.17}$$

where $\Delta d = d - \mathrm{E}\{d\}$. Units of the variance σ_d^2 are the same as units of the squared signal d^2.

The variance is defined in Eq. (2.17) in terms of the expected value of $|\Delta d|^2$ which may be obtained from an average of many images (many realizations) at a particular location r. This is called an *ensemble* average. In practice, it may be necessary to use a *spatial* average of $|\Delta d|^2$ as an estimate of the ensemble average. A system for which the ensemble and spatial averages are equivalent is called *ergodic*. Ergodic systems are discussed later in Section 2.5.5.
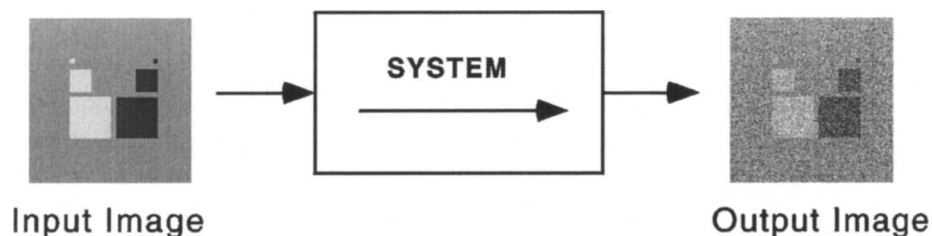
Figure 2.4: Noise in the output image is related to both the noise in the input image and the noise-transfer characteristics of the system. In this example, the image is transferred both with a reduction of image contrast and an increase in image-noise variance.
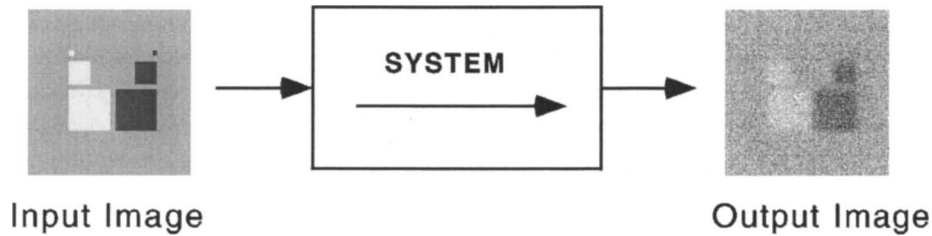
Figure 2.5: A system that degrades spatial resolution and also increases noise will severely compromise image quality as illustrated here, particularly for the visualization of small details.
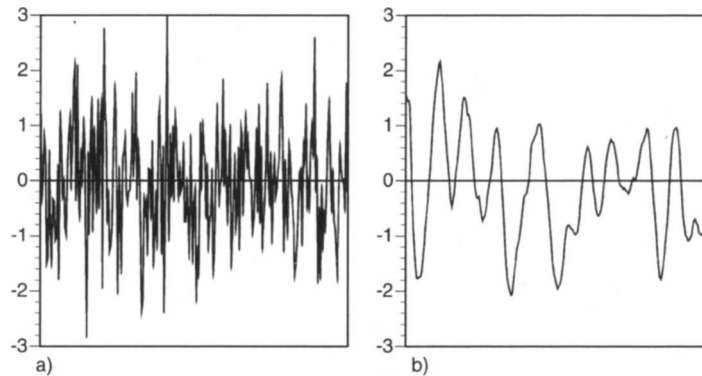
Figure 2.6: One-dimensional profiles may have the same noise variance but look very different as shown here. The noise in b) is correlated over a greater distance than the noise in a).

Figure 2.5 illustrates the input-output relationship of a system that passes contrast in a manner identical to that in Figure 2.3, but increases noise as well. The resulting image quality is severely compromised, and small structures are barely detectable, if at all.

Some insight into system performance could be obtained if a definable relationship existed between the noise variance at the input and output, and the ratio of the two would be the "noise-variance transfer" factor. However, the concept of noise-variance transfer has little meaning for the description of x-ray imaging systems for two reasons. The first is that the variance of an input x-ray quantum image is undefined as described in Section 2.6.2.3. The second is that the variance generally does not describe noise adequately in an analog or digital image. This is illustrated in Figure 2.6. Both profiles have unity noise variance; however, they look very different because the noise in a) is correlated over only a very short distance while noise in b) is correlated over a greater distance. The Fourier transform can be used to describe image noise in the presence of these correlations.
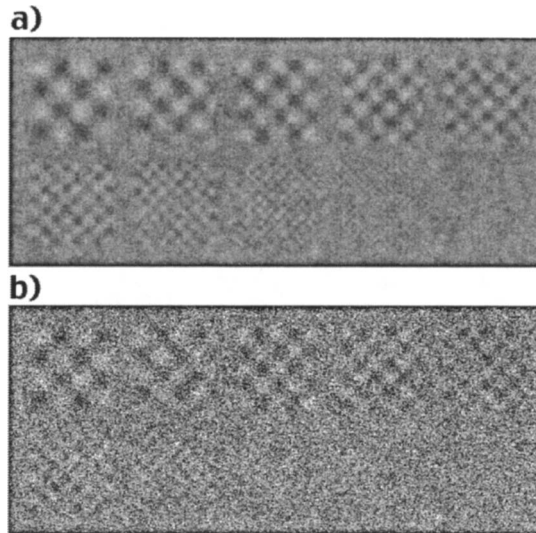
Figure 2.7: The two-dimensional images shown here have the same background noise variance but look very different as the noise in b) is correlated over a greater distance than the noise in a). The same two-dimensional sinusoidal pattern has been added to each image.

2.3 Introduction to linear-systems theory

In this section, linear-systems theory is introduced including a description of important principles and relationships required to characterize system performance in the spatial-frequency domain. While most results are expressed in one-dimensional geometry in terms of the position x and spatial frequency u, similar relationships hold true using two-dimensional geometry in terms of the position vector r and spatial-frequency vector k.

2.3.1 Linear systems

A linear-system response is generally necessary before a linear-systems approach can be used to analyze or characterize system performance. Thus, the first step in any analysis is to ensure the system under study is indeed linear. Essentially, this means the output must be proportional to the input. Thus, if a system has a transfer characteristic described by S{ } such that an input $h(x)$ produces an output S$\{h(x)\}$, then for any two inputs $h_1(x)$ and $h_2(x)$, the system is linear if and only if

$$S\{h_1(x) + h_2(x)\} = S\{h_1(x)\} + S\{h_2(x)\}, \tag{2.18}$$

and

$$S\{ah(x)\} = aS\{h(x)\}, \tag{2.19}$$
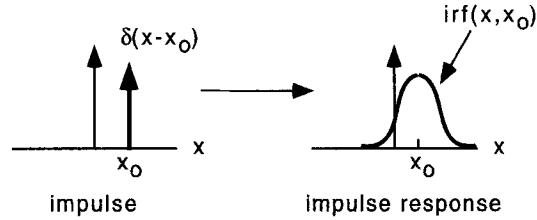
Figure 2.8: An impulse input at $x = x_0$, $\delta(x - x_0)$, produces the impulse-response output irf(x, x_0).
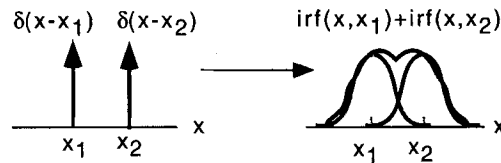
Figure 2.9: For linear systems, the output corresponding to two impulse inputs is the superposition of two impulse-response functions.

for any real constant a. Many systems that are not linear can be linearized with an appropriate calibration, or exhibit small-signal linearity. For instance, radiographic film-screen systems are not linear in their response, but can be linearized if the H&D curve (the relationship between film optical density and x-ray exposure) is known. See references [5], [9], and [20] for further discussions on using linear-systems theory for modeling radiographic systems. In general, no system is completely linear, and as such the linear-systems approach is always an approximation. The analysis of non-linear systems may be limited to their behavior with small amplitude signals [21]. In the following, we will assume a linear system except where specifically noted.

2.3.1.1 Impulse-response function, IRF

When a linear system is presented with the input $\delta(x - x_0)$, an impulse located at $x = x_0$, the corresponding output will be S$\{\delta(x - x_0)\}$ which is called the impulse-response function (IRF), i.e.,

$$\text{irf}(x, x_0) = S\big\{\delta(x - x_0)\big\}. \tag{2.20}$$

The real utility of using the IRF is that for any input expressed as a superposition of many such impulse functions, the output of a linear system will consist of the superposition of one IRF for each input impulse, as shown in Figure 2.8. For instance, if the input is the two impulses shown in Figure 2.9, the output will be

$$S\big\{\delta(x - x_1) + \delta(x - x_2)\big\} = \text{irf}(x, x_1) + \text{irf}(x, x_2). \tag{2.21}$$

There is no requirement that the IRF be isotropic. The IRF is sometimes called the point-spread function (PSF) when used to describe a two-dimensional imaging system.

2.3.2 Linear and shift-invariant (LSI) systems

A system must also have a shift-invariant (isoplanatic) response before a Fourier-based analysis can be used. This requires that the system impulse-response function be shift invariant so that a particular structure in the image will appear the same, regardless of where in the image it is placed. In practice, analysis of systems that are not shift invariant, such as image-intensifier based systems, may be restricted to a central region where the response is approximately shift invariant. A system that is both linear *and* shift invariant in its response is sometimes referred to as an "LSI" system. Because the shape of the IRF in an LSI system is independent of position, it can be written in the form

$$\text{irf}(x, x_0) = \text{irf}(x - x_0). \tag{2.22}$$

2.3.2.1 The convolution integral

If a function $h(x)$ can be approximated as a large number of narrow rectangles having width Δx (see Figure 2.10), the rectangle centered at $x = j\Delta x$, where j is an index identifying the rectangle, has a height $h(j\Delta x)$ and therefore an area $h(j\Delta x) \times \Delta x$. If Δx is small relative to the width of the IRF, the shape of the rectangle is unimportant (only the area is significant) and thus each rectangle can in turn be represented as a δ function, positioned at $x = j\Delta x$, and scaled by $h(j\Delta x) \Delta x$. The output $S\{h(x)\}$ of a system having an IRF described by $\text{irf}(x, x_0)$ can then be expressed approximately as the superposition of an IRF for each delta function:

$$S\{h(x)\} \approx \sum_{j=-\infty}^{\infty} h(j\Delta x)\,\text{irf}(x, j\Delta x)\Delta x. \tag{2.23}$$

In the limit of $\Delta x \to 0$, the summation becomes the integral

$$S\{h(x)\} = \int_{-\infty}^{\infty} h(x')\,\text{irf}(x, x')\,dx', \tag{2.24}$$

which is called a *superposition integral*.

When the IRF is shift invariant, the superposition integral can be simplified to

$$S\{h(x)\} = \int_{-\infty}^{\infty} h(x')\,\text{irf}(x - x')\,dx', \tag{2.25}$$

which is called the *convolution integral* (see Figure 2.11). The convolution integral is of fundamental importance in the imaging sciences (and in many other areas of
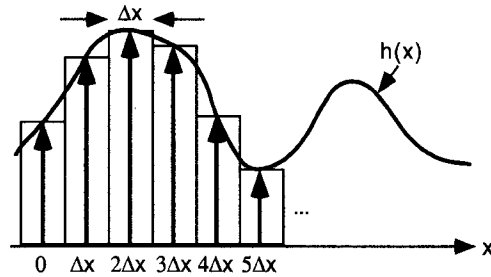
Figure 2.10: An input signal is divided into a large number of narrow rectangles or scaled delta functions, each with area $h(j\Delta x)\Delta x$.

physics, communications theory and engineering). It describes the output signal obtained when the input $h(x)$ is passed through a linear and shift-invariant (LSI) system. The order of the integrands $h(x)$ and irf(x) can be reversed without affecting the outcome. The convolution integral is often expressed in short form as

$$S\{h(x)\} = h(x) * \text{irf}(x). \tag{2.26}$$

Selected properties of the convolution integral are listed in Table 2.2. These should be learned as one learns addition or multiplication, so that they can be used with ease.

It should be noted here that although the convolution integral (Eq. (2.25)) is a standard way of describing the response of an LSI system to an input signal, it describes a *deterministic* system only. That is, a system that has an IRF given *exactly* by irf(x). When the system has a stochastic component in its response, which includes all x-ray imaging systems, it must be viewed as a stochastic system (see Section 2.5.1) and the linear-systems approach using the convolution integral describes only the expectation value of the system response. Image noise can only be described using the linear-systems approach once stochastic theories are included as described in Section 2.5.

2.3.2.2 System characteristic function, T(u)

The IRF contains all the information about a system necessary to determine the expected response in any given situation. However, numerical solutions to the convolution integral are often required in practical situations, and these generally offer little physical insight toward an understanding of system performance. A useful alternative is to examine the special case of an input that varies sinusoidally with position, expressed in terms of the complex exponential

$$h(x) = e^{i2\pi ux} = \cos(2\pi ux) + i\,\sin(2\pi ux), \tag{2.27}$$
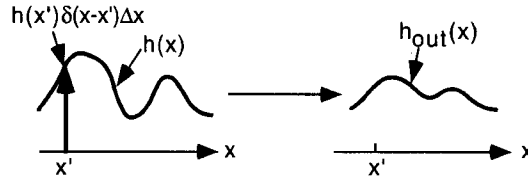
Figure 2.11: For linear and shift-invariant systems the convolution integral describes the superposition of an infinite number of IRF's weighted by the input $h(x)$.

Table 2.2: Properties of the convolution integral

Commutative:
$$f(x) * h(x) = h(x) * f(x)$$
Distributive over Addition:
$$f(x) * [h_1(x) + h_2(x)] = f(x) * h_1(x) + f(x) * h_2(x)$$
Associative:
$$f(x) * h_1(x) * h_2(x) = f(x) * [h_1(x) * h_2(x)]$$
Multiplication with a constant:
$$a[f(x) * h(x)] = af(x) * h(x) = f(x) * ah(x)$$
Addition with a constant:
$$a + [f(x) * h(x)] = [a + f(x)] * h(x) = f(x) * [a + h(x)]$$
Convolution with an impulse:
$$f(x) * \delta(x - x_0) = f(x - x_0)$$

---

where u is the "spatial" frequency (cycles/mm). The output $d(x)$ is given by the convolution integral

$$d(x) = \int_{-\infty}^{\infty} \text{irf}(x')e^{i2\pi u(x-x')}\,dx' \tag{2.28}$$

$$= e^{i2\pi ux} \int_{-\infty}^{\infty} \text{irf}(x')e^{-i2\pi ux'}\,dx', \tag{2.29}$$

where the final integral is recognized as being the Fourier transform of $\text{irf}(x)$, which we call $T(u)$. Therefore,

$$d(x) = S\{e^{i2\pi ux}\} = T(u)e^{i2\pi ux}, \tag{2.30}$$

showing that the output is identical to the input scaled by the frequency-dependent factor $T(u)$. That is, a sinusoidal input will produce a sinusoidal output at the same frequency, scaled by $T(u)$, as illustrated in Figure 2.12. Complex exponentials of the form $e^{i2\pi ux}$ are called *eigenfunctions* of the imaging system, and $T(u)$, which is complex in general, describes the *eigenvalues*. The factor $T(u)$ is called the *characteristic function* of the system. The impulse-response function and the system characteristic function are Fourier pairs:
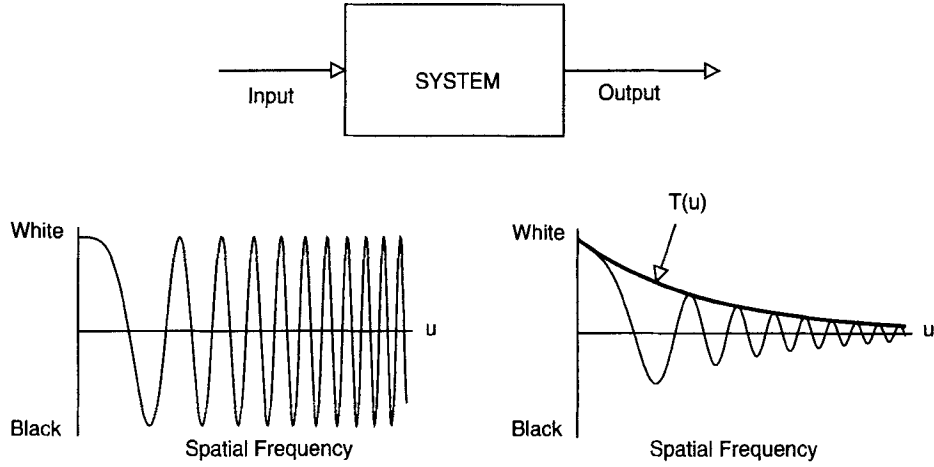
Figure 2.12: A sinusoidal signal at the input of an LSI system will produce a sinusoidal output signal with the same frequency, scaled by the frequency-dependent factor T(u) which is complex in general. This illustration is approximate as the input is not a pure sine wave.

$$T(u) = F\{irf(x)\}. \tag{2.31}$$

This makes it very convenient to use sinusoidal input waveforms to characterize imaging systems.

The Fourier transform expresses a function in terms of its complex sinusoidal-basis components. If a specified input $h(x)$ has the Fourier transform $H(u)$, then $h(x)$ can be expressed as the inverse Fourier transform of $H(u)$ and the corresponding output is

$$d(x) = S\{h(x)\} = S\left\{\int_{-\infty}^{\infty} H(u)e^{i2\pi ux}\,dx\right\} \tag{2.32}$$

$$= \int_{-\infty}^{\infty} H(u)T(u)e^{i2\pi ux}\,du. \tag{2.33}$$

However, because $d(x)$ can also be expressed as the inverse Fourier transform of $D(u)$ where

$$d(x) = \int_{-\infty}^{\infty} D(u)e^{i2\pi ux}\,du, \tag{2.34}$$

we get

$$D(u) = H(u)T(u). \tag{2.35}$$
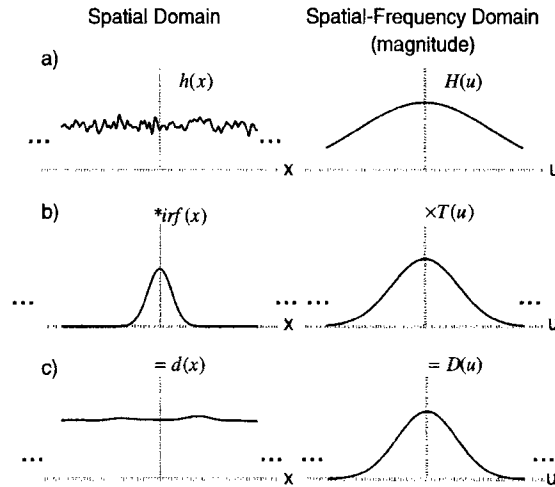
Figure 2.13: Signal-transfer characteristics can be represented either as convolution with irf(x) in the spatial domain (left column) or as multiplication with T(u) in the spatial-frequency domain (right column).

This is a very interesting result because it shows that the Fourier components $H(u)$ of the input are passed unchanged through the system other than a scaling by T(u). Thus, the signal-transfer characteristics of an LSI system can be expressed either as convolution with irf(x) in the spatial domain, or equivalently as multiplication with T(u) in the spatial-frequency domain. This relationship is illustrated graphically in Figure 2.13. In many situations it is more convenient to express imaging problems in the spatial-frequency domain than in the spatial domain, and the ability to move fluently between the two domains is critical to being able to easily solve many imaging problems.

2.3.2.3 Modulation-transfer function, MTF

As shown previously, the contrast-transfer factor, T_c, is not very useful for the description of imaging systems because it is not explicitly related to the size of image structures or to the spatial resolution characteristics of the system. However, the situation changes when we consider the transfer of sinusoidal signals. Consider the input $h(x)$ where

$$h(x) = a + be^{i2\pi ux}, \qquad (2.36)$$

and where the real component of $h(x)$ corresponds to the real (measurable) input signal. Because of the sinusoidal nature of this input, it is more meaningful to characterize it in terms of its modulation than its contrast. The modulation of $h(x)$ in Figure 2.14 is given by

$$M_{in} = \frac{|h_{max}| - |h_{min}|}{|h_{max}| + |h_{min}|} = \frac{(a+b) - (a-b)}{(a+b) + (a-b)} = \frac{b}{a}. \qquad (2.37)$$
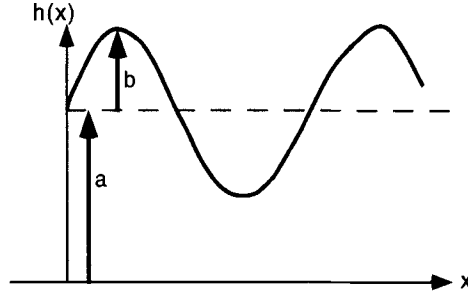
Figure 2.14: A sinusoidal signal expressed in complex exponential form as $h(x) = a + be^{i2\pi ux}$. The sinusoidal waveform is the real component of $h(x)$.

The output signal $d(x)$ is given by

$$d(x) = S\{h(x)\} = S\{a + be^{i2\pi ux}\} \tag{2.38}$$

$$= S\{a\} + S\{be^{i2\pi ux}\} \tag{2.39}$$

$$= aS\{e^{i2\pi(u=0)x}\} + bS\{e^{i2\pi ux}\} \tag{2.40}$$

$$= aT(0) + bT(u)e^{i2\pi ux}, \tag{2.41}$$

where $T(u)$ is complex in general but $T(0)$, which is equal to the area under the IRF, must be real only. The output modulation is therefore given by

$$M_{out} = \frac{|d_{max}| - |d_{min}|}{|d_{max}| + |d_{min}|} = \frac{b}{a} \frac{|T(u)|}{T(0)} = M_{in} \frac{|T(u)|}{T(0)}. \tag{2.42}$$

Similar to our definition above of the contrast-transfer factor, the ratio M_{out}/M_{in} is defined here as the *modulation* transfer function (MTF), given by

$$\text{MTF}(u) = \frac{|T(u)|}{T(0)}, \tag{2.43}$$

where $\text{MTF}(u)$ has by definition a value of unity at $u = 0$.

The MTF is not as complete a description of a system as the characteristic function $T(u)$ because phase information and a scaling constant have been discarded. However, if $\text{irf}(x)$ is real only (i.e., has no imaginary component), which is generally true for x-ray imaging systems, both $T(u)$ and $\text{MTF}(u)$ are even functions and can be expressed in terms of positive frequencies only without loss of generalization. If $\text{irf}(x)$ is real *and* even, $T(u)$ is also real and even, and no phase-transfer information is lost going to the MTF. The MTF is always real.

The function $\text{OTF}(u)$ given by

$$\text{OTF}(u) = \frac{T(u)}{T(0)}, \tag{2.44}$$

is sometimes called the *optical* transfer function (OTF). It is related to the MTF as $\text{MTF}(u) = |\text{OTF}(u)|$, and is similar to the MTF although it retains phase-transfer information.

In general the MTF is a two-dimensional function, expressed in terms of either a two-dimensional frequency vector k as $\text{MTF}(k)$, or orthogonal frequencies u and v as $\text{MTF}(u, v)$.

2.3.2.4 Line-spread function, LSF

The LSF describes the response of the system to a "line" delta function, normalized to unity area. This is seen if we consider a line impulse positioned at $x = x_0$ extending forever in the y direction as the line delta function $\delta(x - x_0)$. The system response along a line in the perpendicular x direction is therefore the LSF given by

$$
\begin{aligned}
\text{lsf}(x - x_0) &= \frac{\displaystyle\int_{-\infty}^{\infty}\int_{-\infty}^{\infty} \delta(x - x_0)\,\text{psf}(x, y)\,\mathrm{d}x\,\mathrm{d}y}{\displaystyle\int_{-\infty}^{\infty}\int_{-\infty}^{\infty} \text{psf}(x, y)\,\mathrm{d}x\,\mathrm{d}y} \\[2em]
&= \frac{\displaystyle\int_{-\infty}^{\infty} \text{psf}(x - x_0, y)\,\mathrm{d}y}{\displaystyle\int_{-\infty}^{\infty}\int_{-\infty}^{\infty} \text{psf}(x, y)\,\mathrm{d}x\,\mathrm{d}y}.
\end{aligned}
\tag{2.45}
$$

For shift-invariant systems this relationship simplifies to

$$
\text{lsf}(x) = \frac{\displaystyle\int_{-\infty}^{\infty} \text{psf}(x, y)\,\mathrm{d}y}{\displaystyle\int_{-\infty}^{\infty}\int_{-\infty}^{\infty} \text{psf}(x, y)\,\mathrm{d}x\,\mathrm{d}y},
\tag{2.46}
$$

where $\text{lsf}(x)$ is the LSF in the x direction. The LSF describes the response of a system in one direction when details of the response in the orthogonal direction have been "integrated out" as shown by Eq. (2.46).

The one-dimensional OTF in Eq. (2.44) and the line-spread function are Fourier pairs [5]:

$$
\text{OTF}(u) = \text{F}\{\text{lsf}(x)\},
\tag{2.47}
$$

where u is the spatial frequency in the x direction. Integration of $\text{psf}(x, y)$ in the y direction in Eq. (2.46) corresponds to evaluation of $\text{MTF}(u, v)$ along the $v = 0$ axis. Therefore,

$$
\text{MTF}(u) = \text{MTF}(u, v)|_{v=0}.
\tag{2.48}
$$

For systems with a rotationally symmetric IRF, MTF(u, v) is also rotationally symmetric and can be expressed in terms of a single radial spatial frequency u without loss of generality.

2.3.2.5 The correlation integral

A quantity closely related to the convolution integral that will also be used later is the correlation integral, not to be confused with the statistical correlation function described in Section 2.5. The correlation integral of two functions $f(x)$ and $h(x)$ is given as

$$d(x', x' + x) = \int_{-\infty}^{\infty} f(x')h(x' + x)\,dx'. \tag{2.49}$$

When $f(x)$ and $h(x)$ are stationary in x, then this relationship simplifies to

$$d(x) = \int_{-\infty}^{\infty} f(x')h(x' + x)\,dx', \tag{2.50}$$

which is written in short form as

$$d(x) = f(x) \star h(x). \tag{2.51}$$

The correlation integral is not commutative, and so

$$f(x) \star h(x) \neq h(x) \star f(x), \tag{2.52}$$

in general. It can also be shown that

$$f(x) \star h(x) = f(x) * h^*(-x) = h(x) * f^*(-x), \tag{2.53}$$

where $h^*(x)$ is the complex conjugate of $h(x)$.

2.4 The spatial-frequency domain

Great emphasis has been placed on being able to solve imaging-physics problems in either the spatial or spatial-frequency domain. The choice is determined by which is easier, and it is often necessary to solve parts of a problem in one domain and other parts in the conjugate domain. In this section, properties of the Fourier transform are described which are invaluable to successfully use this approach.

2.4.1 The Fourier transform

There are several excellent texts describing the Fourier transform including Bracewell [14] and Brigham [15]. See Peters and Williams [22] for a description of the Fourier transform as applied to several concepts in medical imaging.
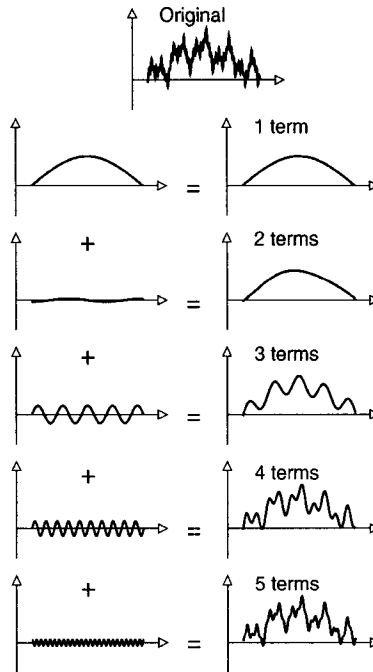
Figure 2.15: The sum of the Fourier components of a function looks more and more like the original function (shown at the top of the figure) as more and more components are added with increasing frequencies. In this figure, five such components are shown in the left-hand column, and the accumulated sum of the components are shown in the right-hand column. In this example, the imaginary terms are all zero.

The Fourier transform of $d(x)$ is $D(u)$, and the inverse Fourier transform of $D(u)$ is again $d(x)$. This reciprocal relationship is expressed by

$$D(u) = \int_{-\infty}^{\infty} d(x)e^{-i2\pi ux}\,dx, \qquad (2.54)$$

$$d(x) = \int_{-\infty}^{\infty} D(u)e^{i2\pi ux}\,du, \qquad (2.55)$$

where u is the spatial frequency along the x axis. It is seen that the units of $D(u)$ will always be those of $d(x) \times x$.

The Fourier transform of $d(x)$ exists for any well-behaved function $d(x)$. Thus, $D(u)$ always exists when $d(x)$ represents some sort of physical quantity, or at least a function which *could* represent a physical quantity, such as image brightness. The Fourier transform of generalized functions also exists, albeit possibly as generalized functions. Thus, the transform of a distribution of quanta exists when each quantum is represented as a δ function, which will be used a great deal later. In general, both $d(x)$ and $D(u)$ are complex, and may be expressed either as a real

Table 2.3: Summary of Fourier-transform relationships in one and two dimensions for LSI systems. $\text{MTF}(u) = |\text{OTF}(u)|$

Spatial Domain	Fourier Transform	Spatial-Frequency Domain
irf(x)	1D	T(u)
lsf(x)	1D	OTF(u)
psf(x, y)	2D	T(u, v)

and imaginary pair, or as a magnitude and phase pair,

$$D(u) = \text{Re}\{D(u)\} + i\,\text{Im}\{D(u)\} \tag{2.56}$$

$$= |D(u)|e^{i\phi(u)}, \tag{2.57}$$

where $\phi(u)$ is the spatial-frequency-dependent phase angle given by

$$\phi(u) = \tan^{-1}\left(\frac{\text{Im}\{D(u)\}}{\text{Re}\{D(u)\}}\right), \tag{2.58}$$

through the Euler-angle relation $e^{i\phi} = \cos\phi + i\sin\phi$.

The Fourier transform expresses the fact that $d(x)$ can be written as the sum of a distribution of sinusoidal components (Figure 2.15). As more components are included, the sum looks more and more like the original function. If all non-zero components are included, the sum is identical to the original.

2.4.1.1   The two-dimensional fourier transform

The two-dimensional Fourier transform of $d(x, y)$, $D(u, v)$, is given by

$$D(u, v) = \int_{-\infty}^{\infty}\int_{-\infty}^{\infty} d(x, y)e^{-i2\pi(ux+vy)}\,dx\,dy, \tag{2.59}$$

and the inverse Fourier transform by

$$d(x, y) = \int_{-\infty}^{\infty}\int_{-\infty}^{\infty} D(u, v)e^{i2\pi(ux+vy)}\,du\,dv. \tag{2.60}$$

These integrals can also be written as vector integrals in terms of the position and frequency vectors r and k as

$$D(k) = \int_{-\infty}^{\infty} d(r)e^{-i2\pi k \cdot r}\,d^2r, \tag{2.61}$$

and

$$d(r) = \int_{-\infty}^{\infty} D(k)e^{i2\pi k \cdot r} \, d^2k. \qquad (2.62)$$

The product $k \cdot r$ is a vector dot product such that $k \cdot r = ux + vy$.

2.4.2 The discrete fourier transform

Manipulation of digital image data in the Fourier domain requires the use of a numerical implementation of the Fourier transform, called a discrete Fourier transform (DFT), which differs from the Fourier transform in subtle ways. The fast Fourier transform (FFT) refers to a number of implementations of the DFT which make use of clever programming to increase computational efficiency. Several implementations of the FFT are available which differ in sophistication, the allowable size and form (real or complex) of the input data sequence, speed of execution, and sometimes a scaler constant.

One commonly used form for the DFT of a sequence of N values d_n for $0 \leqslant n \leqslant N - 1$ is given by

$$D_m = \text{DFT}\{d_n\} = \sum_{n=0}^{N-1} d_n e^{-i2\pi nm/N}, \qquad (2.63)$$

which consists of a sequence of the N complex values D_m for $0 \leqslant m \leqslant N - 1$. The inverse DFT is given by

$$d_n = \text{DFT}^{-1}\{D_m\} = \frac{1}{N} \sum_{m=0}^{N-1} D_m e^{i2\pi nm/N}. \qquad (2.64)$$

Other forms of the DFT exist, differing primarily by a scaler constant of N or $\sqrt{N}$. The user of any DFT should be aware of what DFT algorithm is being used before attempting any quantitative work. We shall use Eqs. (2.63) and (2.64) as definitions of the DFT.

The dimensions of d_n and D_m must necessarily be the same, and they are often dimensionless. This is one way in which the Fourier transform and the discrete Fourier transform differ. Another important consideration when using any DFT is to know which index value (which value of n or m) corresponds to the zero positions $x = 0$ and $u = 0$. In many DFT implementations, the central position $x = 0$ corresponds to $n = N/2 - 1$, while the central frequency $u = 0$ corresponds to $m = 0$. Erroneous placement of the zero position in one domain results in errors in the phase angle of the complex value in the conjugate domain as known from the shift theorem.

When the sequence d_n represents the function $d(x)$ evaluated at uniform spacings x_0, it is sometimes written as $d(nx_0)$ to retain this spatial relevance. However,

this relationship is not as simple in the spatial-frequency domain, as the sequence D_m is *not* equivalent to samples of $D(u)$ at uniform spatial-frequency spacings of $1/Nx_0$, $D(m/Nx_0)$. While it may be tempting to view the DFT as a numerical implementation of the Fourier integral in Eq. (2.55) and write

$$D\left(\frac{m}{Nx_0}\right) = D(u)|_{u=\frac{m}{Nx_0}} \approx x_0 D_m, \qquad (2.65)$$

or

$$D_m \approx \frac{1}{x_0} D\left(\frac{m}{Nx_0}\right), \qquad (2.66)$$

extreme care must be used as the DFT is really a separate transform in its own right. The practical problems associated with this interpretation become clear when the DFT is viewed as a special case of the Fourier transform and is understood in the two domains (Brigham [15]). The problems include:

(a) aliasing;

(b) spectral leakage and side lobes;

(c) truncation and windowing;

(d) zero-position and phase errors (mentioned above);

(e) frequency wrap-around; and,

(f) scaling factors and units (particularly in the frequency domain).

They have been described by various authors. Excellent general works are given by Brigham [15], Bracewell [14], and Peters and Williams [22].

2.4.3 Sampling and aliasing

Many imaging systems of practical importance produce digital images in which image brightness is represented as a sequence of numerical values. In this section, the relationship between a function and its "sampled" (discrete) representation is described in a way that is still amenable to the analytic graphical techniques used previously.

When the function $d(x)$ is represented numerically with the N discrete values d_n for $0 \leqslant n \leqslant N - 1$, each value corresponds to $d(nx_0) = d(x)|_{x=nx_0}$, an evaluation of $d(x)$ at $x = nx_0$. The process of evaluating a function is called "sampling". One way of describing the sampling process is by making use of the sifting property of the δ function, which says that if $d(x)$ is continuous at $x = x_0$, it has a value
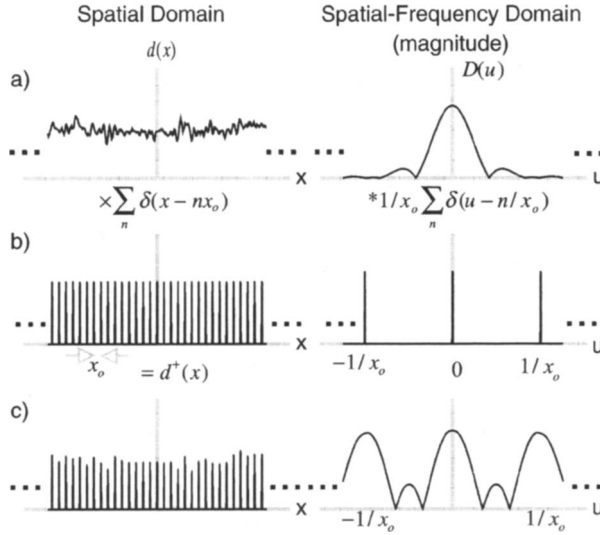
Figure 2.16: Sampling the function $d(x)$ is represented as $d^\dagger(x) = d(x) \sum_{n=-\infty}^{\infty} \delta(x - nx_0)$ and consists of a sequence of δ functions scaled by the discrete values d_n where n is an integer over $-\infty \leqslant n \leqslant \infty$. Spectral aliasing occurs when the aliases overlap in the spatial-frequency domain. Only the magnitude is shown in the frequency domain.

at x_0 given by

$$d(x)|_{x=x_0} = \int_{-\infty}^{\infty} d(x)\delta(x - x_0)\, dx = d(x_0) \int_{-\infty}^{\infty} \delta(x - x_0)\, dx = d(x_0). \quad (2.67)$$

Following Brigham [15], we adopt a graphical representation of this sampling process as shown in Figure 2.16, where each horizontal pair of figures represents a Fourier-transform pair. Sampling $d(x)$ at $x = x_0$ is represented as multiplication with $\delta(x - x_0)$ with the result being an impulse at $x = x_0$ having an undefined amplitude and area equal to $d(x_0)$:

$$d(x)\delta(x - x_0) = d(x_0)\delta(x - x_0). \quad (2.68)$$

This use of the δ function is important because it provides a mechanism whereby sampling can be represented as the linear process of multiplication. This makes it relatively straightforward to interpret the effects of sampling in the conjugate domain.

Note that multiplication with the δ function is not *equivalent* to sampling the function. Rather, multiplication with $\delta(x - x_0)$ results in a δ function positioned at $x = x_0$ that is *scaled* by the sample value of the function. The distinction is important and the δ function cannot be omitted. In addition, the δ function carries the positional information associated with the numerical value.

If a function of infinite extent is sampled at points with uniform spacing x_0, this gives an (infinite) sequence of sample values, $d(nx_0)$ or equivalently d_n, corresponding to values of $d(x)$ at positions $x = nx_0$ where n is an integer. The sampling of a function is therefore represented as multiplication of $d(x)$ with an infinite array of δ functions (Figure 2.16) resulting in $d^\dagger(x)$ where

$$d^\dagger(x) = d(x) \sum_{n=-\infty}^{\infty} \delta(x - nx_0) = \sum_{n=-\infty}^{\infty} d(nx_0)\delta(x - nx_0) \qquad (2.69)$$

$$= \sum_{n=-\infty}^{\infty} d_n \delta(x - nx_0). \qquad (2.70)$$

We use Eqs. (2.69) and (2.70) as our definition of sampling, where $d(x)$ is called the "presampling" signal and $d^\dagger(x)$ is a sequence of scaled δ functions. Note that this definition of sampling does not represent a physical measurement process, only the evaluation of a function. A physical measurement would require the use of a sampling function having finite spatial extent that would reflect the spatial sensitivity of the detector as used in Section 2.2.4 in the description of distribution theory. The δ function can be interpreted as an "ideal" sampling function having infinitesimal width.

The function $d^\dagger(x)$ is also referred to as a pulse-amplitude modulated (PAM) signal, consisting of a sum of modulated pulses at uniform spacings x_0. Many important concepts used to describe digital images come from the electronic communication field, where signals are sampled at uniform time intervals rather than uniform space intervals.

A comment on units is warranted here. A δ function has units equal to the inverse of its argument—see Eq. (2.11). In Eq. (2.69), $\delta(x - nx_0)$ therefore has dimensions of length^{-1} and hence $d^\dagger(x)$ has dimensions equal to those of $d(x) \times x^{-1}$ which are different from those of $d(x)$.

The effect of spatial sampling in both the spatial and spatial-frequency domains is shown in Figure 2.16, where each graph in the right column is the Fourier transform of the corresponding graph in the left. Multiplication in the x domain corresponds to convolution in the u domain. Thus, the Fourier transform of $d^\dagger(x)$, as shown in the lower right of Figure 2.16, is given by

$$F\{d^\dagger(x)\} = D(u) * \frac{1}{x_0} \sum_{n=-\infty}^{\infty} \delta\left(u - \frac{n}{x_0}\right), \qquad (2.71)$$

where $D(u)$ is the Fourier transform of $d(x)$. The Fourier transform of $d^\dagger(x)$ therefore consists of $D(u)$ scaled by $1/x_0$ and superimposed with an infinite number of similarly scaled aliases of $D(u)$ centered at frequencies $u = n/x_0$. As shown in Figure 2.16, the aliases may overlap if $D(u)$ extends beyond $u = \pm 1/2x_0$ where $1/x_0$ is the "sampling frequency," and $1/2x_0$ is called the sampling "cutoff frequency." If aliasing occurs, the true Fourier transform $D(u)$ cannot be determined

from the aliased Fourier transform alone. This is equivalent to saying that the original function $d(x)$ cannot be determined from the sample values $d(nx_0)$ alone once aliasing has occurred.

2.4.3.1 The sampling theorem

The above considerations lead directly to a statement of the sampling theorem, adapted from Bracewell [14]:

> Any band-limited function having infinite extent and no component frequencies at frequencies greater than $u = u_{max}$ can be fully determined from an infinite set of discrete samples if sampled at a frequency greater than $u_{Ny} = 2u_{max}$ where u_{Ny} is called the Nyquist sampling frequency.

This is just the condition to prevent overlap of the aliases in Figure 2.16. An even function (e.g., a cosine wave relative to the sampling grid) can be fully determined when sampled right at the Nyquist frequency, but an odd function (e.g., a sine wave relative to the sampling grid) must be sampled slightly above the Nyquist frequency. As a rule of thumb, it is wise to sample at a frequency greater than the Nyquist sampling frequency, such as u_s given by

$$u_s = f_k \times u_{Ny} = f_k \times 2u_{max},$$
(2.72)

where $f_k \approx 1.2$ is an empirically determined constant called the "Kell" factor.

2.4.3.2 Recovering a continuous function from sample values

The question should be asked whether the original presampling function $d(x)$ can be recovered exactly from the sample values d_n. In the conjugate domain this question is equivalent to asking whether $D(u)$ can be recovered exactly from the aliased spectrum $F\{d^\dagger(x)\}$ in the lower right of Figure 2.16. In the absence of aliasing such that there is no overlap of the aliases, the original primary spectral component can indeed be isolated from its aliases by multiplication with the rectangular function $x_0\Pi(x_0u)$ having a value x_0 over $-1/2x_0 \leqslant u \leqslant 1/2x_0$ and zero elsewhere where x_0 is the sample spacing. This rectangular function has an inverse Fourier transform $\mathrm{sinc}(\pi x/x_0)$, and hence the recovered signal $\hat{d}(x)$ is obtained as a convolution of $d^\dagger(x)$ with the sinc-function

$$\hat{d}(x) = d^\dagger(x) * \mathrm{sinc}(\pi x/x_0)$$
(2.73)

$$= \int_{-\infty}^{\infty} \sum_{n=-\infty}^{\infty} d_n\delta(x' - nx_0)\,\mathrm{sinc}\left(\pi\frac{x-x'}{x_0}\right)\mathrm{d}x'$$
(2.74)

$$= \sum_{n=-\infty}^{\infty} d_n \int_{-\infty}^{\infty} \delta(x' - nx_0)\,\mathrm{sinc}\left(\pi\frac{x-x'}{x_0}\right)\mathrm{d}x'$$
(2.75)

Spatial Domain   Spatial-Frequency Domain
                            (magnitude)

a)

$d^+(x)$

$-2x_o$ $-x_o$ 0 x_o $2x_o$

b) $*\mathrm{sinc}(\pi x /x_o)$

x_o

$-1/2x_o$ $1/2x_o$

c) $= \hat{d}(x)$ $= \hat{D}(u)$
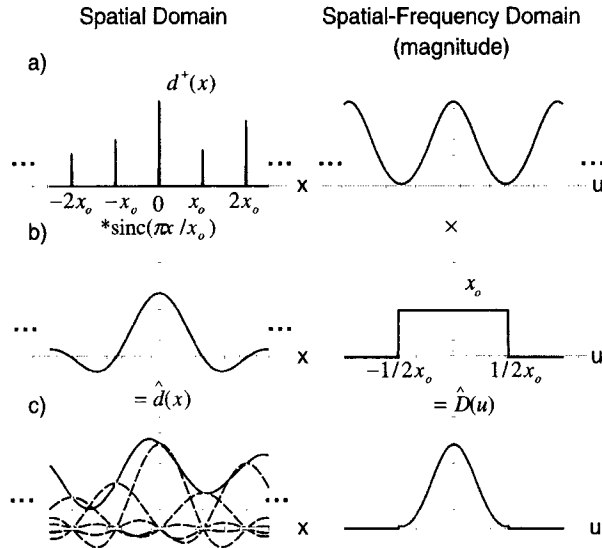
Figure 2.17: The recovered function $\hat{d}(x)$ is obtained by convolving $d^\dagger(x)$ with $\mathrm{sinc}(\pi x/x_0)$, resulting in the superposition of a scaled sinc function for each sampled point as indicated by the dashed lines in c). Only the magnitude is shown in the frequency domain.

$$= \sum_{n=-\infty}^{\infty} d_n \,\mathrm{sinc}\!\left(\pi\,\frac{x - nx_0}{x_0}\right),\qquad (2.76)$$

again using the sifting theorem. Convolution of the sample values with the sinc function is sometimes referred to as sinc interpolation.

Thus, as illustrated in Figure 2.17, recovering the continuous function is achieved by the superposition of a series of scaled sinc functions corresponding to each sampled valued. Each sinc function has a value of zero at positions corresponding to all other sample locations, and hence the value of $\hat{d}(x)$ is still equal to $d(x)$ for $x = nx_0$. Use of the sampled function $d^\dagger(x)$ with δ functions is key to enabling this elegant representation.

The recovered continuous function $\hat{d}(x)$ is exactly equal to the original presampling function $d(x)$ *only* if there is no aliasing resulting from the sampling process. Aliasing would correspond to an overlap of the central component with the shifted spectral aliases (as illustrated in Figure 2.16) which could therefore not normally be isolated from the aliases.

2.5 Stochastic processes in linear systems

A random (stochastic) process can be viewed here as any mechanism giving rise to random fluctuations in a signal, generally represented as a random variable. It is not possible to precisely predict the future values of a random variable, but it may be possible to determine its statistical properties. Excellent general references for a description of stochastic processes are Papoulis [17] or Bendat and Piersol [16].

In this section, the mathematical tools required to characterize noise in medical imaging systems are summarized.

2.5.1 Deterministic versus stochastic systems

A distinction can be made between deterministic systems and stochastic systems [17]. A deterministic system, when presented with two identical inputs, will produce *exactly* the same output both times. There will be absolutely no difference, even under close examination. On the other hand, a stochastic system, when presented with two identical inputs, may produce similar outputs but they will not be exactly the same. There are many reasons why the two sample outputs may differ. For instance, some systems may use secondary image quanta (e.g., light generated in a screen, electron-hole pairs in a detector, etc.) to transfer the image from input to output, and the statistical properties of these quanta may introduce a random component in the output image. These systems are therefore fundamentally stochastic systems, independent of the statistical properties of the incident x-ray quanta.

2.5.2 Expected value and variance

The simplest way of characterizing a random variable is in terms of its expected value and variance. The expected value of the random variable a is $E\{a\}$ given by [17]

$$E\{a\} = \int_{-\infty}^{\infty} \alpha \lambda_a(\alpha) \, d\alpha, \qquad (2.77)$$

where $\lambda_a(\alpha)$ is the probability of a having the value α. The variance expresses the expected value of the squared deviation from the expected value, given by [17]

$$\sigma_a^2 = E\{|\Delta a|^2\} = E\{|a - E\{a\}|^2\} = E\{a^2\} - |E\{a\}|^2, \qquad (2.78)$$

where $\Delta a = a - E\{a\}$.

2.5.3 Autocorrelation and autocovariance

If $a(x)$ is a complex random variable expressed as a function of x, the autocorrelation of $a(x)$ is $R_a(x', x' + x)$ given by [17]

$$R_a(x', x' + x) = E\{a(x')a^*(x' + x)\}, \qquad (2.79)$$

where $*$ indicates a complex conjugate. When $a(x)$ is a real-only value, $a^*(x) = a(x)$. The autocorrelation describes the correlation of $a(x')$ with itself at a location displaced by x.

The autocovariance describes the correlation of $a(x')$ with itself at a location displaced by x about the expected values. Thus, the autocovariance of the random variable $a(x)$ is [17]

$$K_a(x', x' + x) = E\{\Delta a(x')\Delta a^*(x' + x)\} \tag{2.80}$$

$$= R_a(x', x' + x) - E\{a(x')\}E\{a^*(x' + x)\}. \tag{2.81}$$

2.5.4 Wide-sense stationary (WSS) random processes

If a is a real-valued random variable for which the expected value and variance are stationary, that is, have fixed values, the expected value $E\{a\}$ is given by the sample mean in the limit of $N \to \infty$,

$$E\{a\} = \lim_{N \to \infty} \frac{1}{N} \sum_{n=1}^{N} a_n, \tag{2.82}$$

where a_n is the nth value of a, and the variance by

$$\sigma_a^2 = \lim_{N \to \infty} \frac{1}{N} \sum_{n=1}^{N} (a_n - E\{a\})^2 \tag{2.83}$$

$$= \lim_{N \to \infty} \frac{1}{N-1} \left[\sum_{n=1}^{N} a_n^2 - \frac{1}{N} \left(\sum_{n=1}^{N} a_n \right)^2 \right]. \tag{2.84}$$

A random process in x having all statistical properties stationary with x is called *strict-sense stationary* (SSS). A process having at least the expected value and autocorrelation stationary in x is called *wide-sense stationary* (WSS). For instance, if $a(x)$ is a WSS random process, the autocorrelation in Eq. (2.79) depends on the separation x, but not on the position x'. This simplification means that [17]

$$R_a(x', x' + x) = R_a(x), \tag{2.85}$$

and

$$K_a(x', x' + x) = K_a(x). \tag{2.86}$$

If $a(x)$ is a real process, $R_a(x)$ and $K_a(x)$ are real and even.

2.5.4.1 Noise power spectrum of a WSS random process

The autocovariance of a WSS random process, $K_a(x)$, provides a complete description of the second-order second-moment statistics in the spatial domain. In the spatial-frequency domain, the same statistics are described by the Wiener spectrum, equal to the Fourier transform of the autocovariance function. The Wiener

spectrum describes the spectral decomposition of the noise variance of a WSS random process. That is, it describes the contribution to the variance from spatial frequencies between u and $(u + du)$.

For historical reasons, the Wiener spectrum is also called the noise-power spectrum (NPS). This resulted from the fact that if $a(t)$ represents a random (in time) voltage fluctuation across a pure resistance of one ohm, the expected average power dissipated by the resistance is given by the variance of $a(t)$. Thus, the spectral decomposition of the variance is called the power spectrum, or noise power spectrum, or sometimes the covariance spectrum [17].

In an imaging context, the NPS of a random process $a(x)$, $\text{NPS}_a(u)$, is expressed as a function of spatial frequencies (u) rather than temporal frequencies (t), and can be written in terms of the autocovariance as

$$\text{NPS}_a(u) = \text{F}\{\text{K}_a(x)\}. \tag{2.87}$$

Thus, the NPS and the autocovariance of a WSS random process are Fourier-transform pairs. If $a(x)$ is a real function, $\text{NPS}_a(u)$ is real and even.

2.5.5 Ergodic WSS random processes

Use of Eqs. (2.80) to characterize image noise requires the expected values $\text{E}\{a(x)\}$ and $\text{E}\{a(x')a^*(x' + x)\}$ for each x value, which may be difficult or impossible to obtain in practice. Fortunately, many random processes responsible for noise in medical imaging systems are ergodic or can be approximated as being ergodic. Being ergodic means that expected values can be determined equivalently from *ensemble* averages or *spatial* averages [17]. Thus, while the autocovariance is given by Eq. (2.80) based on true expectation values, an estimate of the autocovariance for a WSS mean ergodic random process is given by the *sample autocovariance*, $\text{K}_{a,X}(x)$, which is a spatial average,

$$\text{K}_{a,X}(x) = \frac{1}{X} \int_X \Delta a(x')\Delta.a^*(x' + x)\,dx' \tag{2.88}$$

In the limit of $X \to \infty$, the sample covariance gives the autocovariance:

$$\text{K}_a(x) = \lim_{X \to \infty} \text{K}_{a,X}(x) \tag{2.89}$$

$$= \lim_{X \to \infty}\left[\frac{1}{X} \int_X a(x')a^*(x' + x)\,dx' \right.$$

$$\left. - \frac{1}{X} \int_X a(x')\,dx' \frac{1}{X} \int_X a^*(x' + x)\,dx'\right] \tag{2.90}$$

$$= \lim_{X \to \infty} \frac{1}{X} \int_X \Delta a(x')\Delta a^*(x' + x)\,dx' \tag{2.91}$$

$$= \Delta a(x) \star \Delta a^*(x), \tag{2.92}$$

where $\star$ represents the correlation operation.

2.5.5.1 Noise power spectrum of an ergodic WSS random process

The NPS of a WSS random process is given by Eq. (2.87), and $K_a(x)$ for a WSS ergodic random process is given by Eq. (2.91). From this it can be shown that the NPS of a WSS ergodic random process is given by

$$\text{NPS}_a(u) = \lim_{X \to \infty} \frac{1}{X} \text{E}\left\{ \left| \int_X \Delta a(x) e^{-i2\pi u x} \, dx \right|^2 \right\} \qquad (2.93)$$

$$= \lim_{X \to \infty} \frac{1}{X} \text{E}\left\{ \left| F_X\{\Delta a(x)\} \right|^2 \right\}, \qquad (2.94)$$

where $F_X\{\Delta a(x)\}$ is the Fourier transform of the zero-mean function $\Delta a(x)$ truncated to the region $-X/2 \leqslant x \leqslant X/2$. Equations (2.87) and (2.94) can each be used to determine the NPS of a WSS ergodic random process. The units of $\text{NPS}_a(u)$ are equal to those of $a^2(x) \times x$.

The variance of an ergodic WSS random process $a(x)$ is given by

$$\sigma_a^2 = \text{E}\{a(x)a^*(x)\} - \text{E}\{a(x)\}\text{E}\{a^*(x)\} \qquad (2.95)$$

$$= \text{E}\{\Delta a(x)\Delta a^*(x)\} \qquad (2.96)$$

$$= K_a(x)|_{x=0}, \qquad (2.97)$$

and therefore the Fourier DC theorem shows that the variance of $a(x)$ can also be written in terms of the NPS as

$$\sigma_a^2 = \int_{-\infty}^{\infty} \text{NPS}_a(u) \, du. \qquad (2.98)$$

In summary, use of Fourier-based descriptions of image noise requires two important assumptions. The first is that processes responsible for noise both in the input signal and within the imaging chain be wide-sense stationary (WSS). This means that the mean and autocovariance of the noise processes, and the second-order noise-transfer characteristics of the imaging system, are stationary in x. This condition is often satisfied for the analysis of noise in low-contrast imaging tasks. The second assumption is that the system be ergodic. While it can be difficult to prove ergodicity, many systems of practical importance can be considered ergodic if practical approximations are made. For instance, the expectation values of image-intensifier-based video systems can be determined from multiple sequential video frames and the system can be considered ergodic if the analysis is restricted to central regions of the image. Stimulable phosphor or film-screen-based systems have grain noise that is not ergodic, and which may have to be addressed as a separate noise source.

2.5.6 Ergodic wide-sense cyclostationary (WSCS) random processes

Another important category of stochastic processes are those that exhibit some periodic behavior but which have statistical properties that are still invariant to a shift of any multiple of that period (Papoulis [17], Gardner and Franks [23]). A process is called *strict-sense cyclostationary* (SSCS) with period x_0 if all its statistical properties are invariant to a shift of nx_0 for any integer n, and *wide-sense cyclostationary* (WSCS) if only the mean and correlation are invariant. Thus, $a(x)$ is WSCS with period x_0 if

$$E\{a(x + nx_0)\} = E\{a(x)\}, \tag{2.99}$$

and

$$R_a(x' + nx_0, x' + x + nx_0) = R_a(x', x' + x), \tag{2.100}$$

for any integer n. In imaging, an important type of cyclostationary process is that which can be written in the form

$$a(x) = \sum_{n=-\infty}^{\infty} a_n s(x - nx_0), \tag{2.101}$$

where $s(x)$ is called the *sensing* function of the WSCS process. The expected value of $a(x)$ is given by

$$E\{a(x)\} = E\{a_n\} \sum_{n=-\infty}^{\infty} s(x - nx_0), \tag{2.102}$$

where $E\{a_n\}$ is the expected value of a_n. For WSCS ergodic random processes, the autocorrelation is given by

$$R_a(x) = \frac{1}{x_0} \sum_{n=-\infty}^{\infty} R_a(nx_0)\tau(x), \tag{2.103}$$

where

$$\tau(x) = \int_{-\infty}^{\infty} s(x')s(x' + x)\,dx' = s(x) \star s(x). \tag{2.104}$$

Wide-sense cyclostationary ergodic random processes are important in the description of digital-imaging systems. For instance, if $a(x)$ is a WSS ergodic stochastic process that is represented with the digital samples $a_n = a(nx_0)$ obtained

using impulse sensing functions at uniform spacing x_0, $s(x) = \sum_{n=-\infty}^{\infty} \delta(x - nx_0)$, then $a^{\dagger}(x)$, given by

$$a^{\dagger}(x) = \sum_{n=-\infty}^{\infty} a_n \delta(x - nx_0), \qquad (2.105)$$

is an infinite train of amplitude-modulated δ functions and is a WSCS ergodic random process with period x_0. The expected value of $a^{\dagger}(x)$ is given by [17, 23]

$$E\{a^{\dagger}(x)\} = E\{a_n\} \sum_{n=-\infty}^{\infty} \delta(x - nx_0). \qquad (2.106)$$

The autocorrelation of $a^{\dagger}(x)$, $R_{a^{\dagger}}(x)$, is given by

$$R_{a^{\dagger}}(x) = \frac{1}{x_0} \sum_{n=-\infty}^{\infty} R_a(nx_0)\delta(x - nx_0) = \frac{1}{x_0} R_a(x) \sum_{n=-\infty}^{\infty} \delta(x - nx_0), \qquad (2.107)$$

where $R_a(x)$ is the autocorrelation of $a(x)$. Similarly, the autocovariance, $K_{a^{\dagger}}(x)$, is given by

$$K_{a^{\dagger}}(x) = \frac{1}{x_0} \sum_{n=-\infty}^{\infty} K_a(nx_0)\delta(x - nx_0) = \frac{1}{x_0} K_a(x) \sum_{n=-\infty}^{\infty} \delta(x - nx_0), \qquad (2.108)$$

where $K_a(x)$ is the autocovariance of $a(x)$. The units of $K_{a^{\dagger}}(x)$ are equal to those of $a^2(x) \times x^{-2}$.

2.5.6.1   Noise-power spectrum of an ergodic WSCS random process

In the previous section, $NPS_a(u)$ was introduced as the NPS of a WSS random process, given by the Fourier transform of the autocovariance of that random process. Following Gardner and Franks [23], we introduce $NPS_{a^{\dagger}}(u)$ as the Fourier transform of $K_{a^{\dagger}}(x)$, the autocovariance of the WSCS random process $a(x)$ is given by

$$NPS_{a^{\dagger}}(u) = F\{K_{a^{\dagger}}(x)\} \qquad (2.109)$$

$$= \frac{1}{x_0^2} NPS_a(u) * \sum_{n=-\infty}^{\infty} \delta\left(u - \frac{n}{x_0}\right), \qquad (2.110)$$

with units of $a^2(x) \times x^{-1}$. It is important to note that these units are different from those of $NPS_a(u)$, which are $a^2(x) \times x$.

This result shows that the NPS of a random-process periodic in the spatial domain with period x_0 is periodic also in the spatial-frequency domain with period $1/x_0$. This has important implications when used to describe noise in digital-imaging systems which may suffer from noise aliasing (Section 2.9.3).

2.6 Metrics of system performance

The stochastic nature of image quanta imposes a fundamental limitation on the performance of imaging systems, and gives rise to stochastic fluctuations in the image signals contributing to image formation. In this section, metrics developed to describe image quality in terms of signal and noise are described within a linear-systems framework.

2.6.1 Rose model signal-to-noise ratio

The importance of the statistical nature of image quanta to imaging was first recognized in 1948 by Rose [2, 3] and his contemporaries [24–26], and their work forms the basis of many introductory texts on the nature of signal and noise in radiography. The relationship between the number of image quanta and perception of detail is embodied in the "Rose Model," as it has come to be known, describing the signal-to-noise ratio (SNR) for the detection of a uniform object in a uniform background having a mean $\overline{q}_b$ quanta per unit area. If $\overline{q}_0$ is the mean number of quanta per unit area in the region of the object, the resulting contrast C can be written as

$$C = (\overline{q}_b - \overline{q}_0)/\overline{q}_b. \tag{2.111}$$

Rose defined "signal" to be the *incremental change* in the number of image quanta caused by to the object integrated over the area of that object. This is different from the definition of signal used elsewhere in this chapter, and hence we will call his signal the "Rose signal," ΔS_{Rose}, or difference signal, where

$$\Delta S_{Rose} = (\overline{q}_b - \overline{q}_0)A, \tag{2.112}$$

for a uniform object of area A. The noise in Rose's signal is the standard deviation in the number of quanta in an equal area of uniform background, σ_b. For the special case of uncorrelated background quanta, noise is described by Poisson statistics and $\sigma_b = \sqrt{A\overline{q}_b}$ so that the Rose SNR, ΔSNR_{Rose}, is given by

$$\Delta SNR_{Rose} = \frac{A(\overline{q}_b - \overline{q}_0)}{\sqrt{A\overline{q}_b}} = C\sqrt{A\overline{q}_b}. \tag{2.113}$$

Rose showed that ΔSNR_{Rose} must have a value of approximately five or greater for reliable detection of a uniform object under these conditions.

This result led to the general expectation that lesion detectibility should be proportional to object contrast and to the square root of object area and radiation dose (at a single x-ray energy). Under the Rose conditions (uniform object, uniform background, and uncorrelated Poisson-distributed noise), this relationship is found to be approximately correct. For instance, Figure 2.18 shows an image of a contrast-detail phantom obtained using a prototype digital x-ray mammography detector. Examination of this image shows that detectibility of these low-contrast

lesions increases with lesion diameter (square root of area) and contrast, consistent with the Rose model.

Some implications and limitations of the Rose model are described in terms of modern detection theory by Burgess [27]. He shows that the Rose model corresponds to the very specific detection task called "signal known exactly" (SKE) and "background known exactly" (BKE) detection task [27, 28].

The Rose model played an essential role in establishing the fact that image quality is ultimately limited by the statistical nature of image quanta. However, its limitations quickly become apparent when used to assess image quality in many practical situations. The primary restriction is the definition of noise used by Rose in Eq. (2.113), which is valid only for uncorrelated Poisson-distributed noise. In general, noise in a recorded image is neither uncorrelated nor Poisson distributed. This may be because of the presence of additive system noise (e.g., electronic or film noise), quantum amplification stages in a cascaded system (described later), or statistical correlations introduced into the image signals by the scatter of x rays or secondary image quanta in the detector system (e.g., light in a radiographic screen). For all of these reasons, the original Rose model needs appropriate extension and elaboration to be of practical value in the analysis of most modern medical-imaging systems. The use of Fourier-based metrics of image signal and noise facilitates this extension.
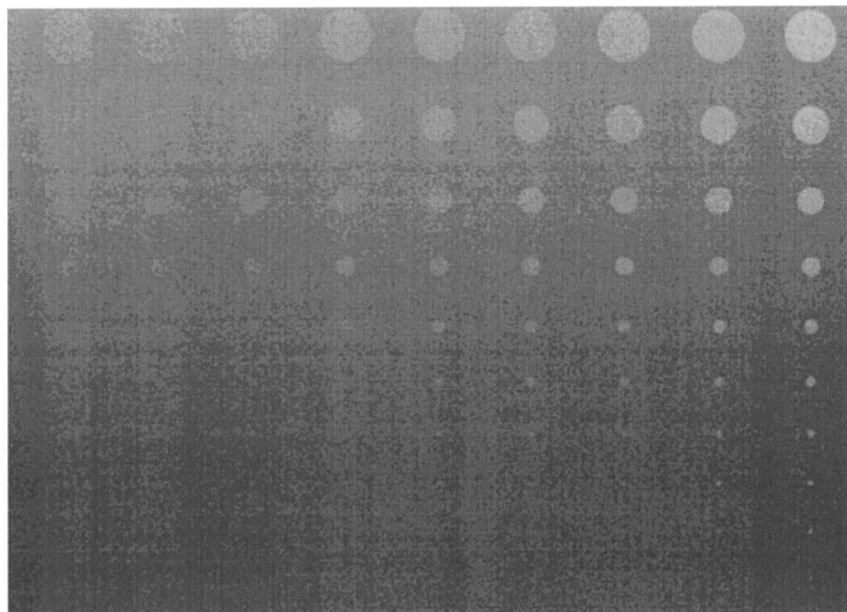

Figure 2.18:   Image of a contrast-detail test phantom obtained with a prototype digital x-ray mammography detector. Lesion contrast increases in the horizontal direction and lesion diameter increases in the vertical direction (courtesy M. Yaffe).

2.6.2 Noise-power spectrum (NPS) and variance

The NPS of a one-dimensional random process $d(x)$, $NPS_d(u)$, is given by Eq. (2.87) for a WSS random process, and by Eqs. (2.87) or (2.93) for an ergodic WSS random process. Thus, $NPS_d(u)$ has units of $d^2(x) \times x$.

The NPS of a two-dimensional ergodic WSS random process $d(x, y)$, $NPS_d(u, v)$, is given by

$$NPS_d(u, v)$$

$$= \lim_{X,Y \to \infty,\infty} \frac{1}{XY} E\left\{ \left| \int_X \int_Y \Delta d(x, y) e^{-i2\pi(ux+vy)} \, dx \, dy \right|^2 \right\} \qquad (2.114)$$

$$= \lim_{X,Y \to \infty,\infty} \frac{1}{XY} E\left\{ \left| F_{X,Y}\{\Delta d(x, y)\} \right|^2 \right\} \qquad (2.115)$$

$$= \lim_{X,Y \to \infty,\infty} E\left\{ S_{\Delta d, X, Y}(u, v) \right\}, \qquad (2.116)$$

where $F_{X,Y}\{d(x, y)\}$ is the Fourier transform of $d(x, y)$ truncated to the region $-X/2 \leqslant x \leqslant X/2, -Y/2 \leqslant y \leqslant Y/2$, and $S_{\Delta d, X, Y}(u, v)$ is the two-dimensional sample spectrum of $\Delta d(x, y)$ over the same range. The units of $NPS_d(u, v)$ are equal to those of $d^2(x, y) \times x^2$.

2.6.2.1 NPS in one and two dimensions

While a two-dimensional analysis of the NPS is sometimes necessary [29], visualization in two dimensions can be problematic. In many situations it is adequate to examine the two-dimensional NPS in only one specified direction at a time (which we will call the x direction with corresponding spatial frequency u), where the dependence in the perpendicular direction has been removed by integration. For instance, if we define $d_Y(x)$ as the integral of $d(x, y)$ over a distance Y in the y direction, then

$$d_Y(x) = \int_Y d(x, y) \, dy, \qquad (2.117)$$

and the NPS of $d_Y(x)$, $NPS_{d_Y}(u)$, is given by

$$NPS_{d_Y}(u)$$

$$= \lim_{X,Y \to \infty,\infty} E\left\{ \frac{1}{XY} \left| \int_X \Delta d_Y(x) e^{-i2\pi ux} \, dx \right|^2 \right\} \qquad (2.118)$$

$$= \lim_{X,Y \to \infty,\infty} E\left\{ \frac{1}{XY} \left| \int_X \left[\int_Y \Delta d(x, y) e^{-i2\pi(ux+vy)} \, dy \right]_{v=0} dx \right|^2 \right\}, (2.119)$$

which is the two-dimensional NPS of $d(x, y)$ evaluated along the $v = 0$ axis. Therefore,

$$\text{NPS}_{d_Y}(u) = \text{NPS}_d(u, v)|_{v=0}. \tag{2.120}$$

Thus, the NPS of a two-dimensional random process, $d(x, y)$, whether expressed as a one-dimensional or two-dimensional NPS, will have the units of $|d(x, y)|^2 \times x^2$. The NPS of both analog and digital images is generally expressed in units of mm^2.

The NPS and the autocovariance are Fourier pairs. The autocovariance of $d_Y(x)$ is therefore related to that of $d(x, y)$ by

$$K_{d_Y}(x) = \lim_{Y \to \infty} \frac{1}{Y} \int_Y K_d(x, y)\, dy, \tag{2.121}$$

as a direct consequence of the central-slice theorem.

2.6.2.2 The zero-frequency value of the NPS

The value of $\text{NPS}_a(u)$ for $u = 0$ is called the zero-frequency, or scale, value of the NPS. Using the Fourier DC theorem and Eq. (2.87), the zero-frequency value can be written as the autocovariance integrated over all x:

$$\text{NPS}_a(u)|_{u=0} = \int_{-\infty}^{\infty} K_a(x)\, dx \tag{2.122}$$

$$= \int_{-\infty}^{\infty} E\{\Delta a(x')\Delta a(x' + x)\}\, dx. \tag{2.123}$$

The zero-frequency value of $\text{NPS}_a(u)$ therefore depends on the extent to which $\Delta a(x)$ may be correlated.

To facilitate further analysis, it is useful to define an average correlation length of the random process $a(x)$, X_{cor}. It is defined such that if $a(x)$ has the autocovariance $K_a(x)$, the area of the rectangle formed by X_{cor} and $K_a(0)$ is the same as that
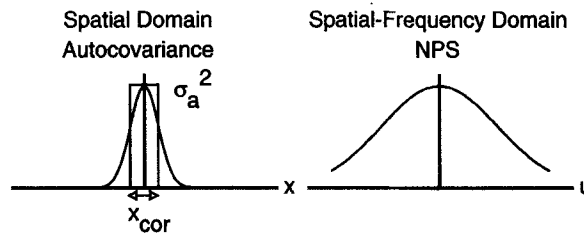
Figure 2.19: The average correlation length of $a(x)$ is defined as X_{cor}, the effective width of the autocovariance function $K_a(x)$ forming a rectangle with the same area as $K_a(x)$.

of $K_a(x)$, as illustrated in Figure 2.19. That is,

$$\int_{-\infty}^{\infty} K_a(x)\,dx = X_{cor}K_a(0).\tag{2.124}$$

The value $K_a(0)$ is equal to the variance σ_a^2, and hence combining this result with Eq. (2.122) gives

$$NPS_a(u)|_{u=0} = X_{cor}\sigma_a^2.\tag{2.125}$$

In an analogous way, the zero-frequency value of a two-dimensional NPS is given as

$$NPS_a(u,v)|_{u,v=0,0} = \iint_{A_{cor}} \sigma_a^2\,dx\,dy = A_{cor}\sigma_a^2,\tag{2.126}$$

where A_{cor} is the two-dimensional average correlation area.

An important special case occurs when measurements are made of a random process, such as variations in optical density of an exposed film. For instance, if $OD(x, y)$ describes the "true" optical density at position (x, y), measurements of film density obtained using a rectangular aperture (sampling function) with dimensions X by Y and area $A = XY$ can be written as $d(x, y)$ where

$$d(x,y) = \frac{1}{A}\int_{x-X/2}^{x+X/2}\int_{y-Y/2}^{y+Y/2} OD(x,y)\,dx'\,dy'$$

$$= \frac{1}{A}OD(x,y) * \prod\left(\frac{x}{X}, \frac{y}{Y}\right).\tag{2.127}$$

As will be shown in Section 2.7.2, the NPS of $d(x, y)$ is therefore given by

$$NPS_d(u,v) = NPS_{OD}(u,v)\left|\text{sinc}(\pi Xu)\text{sinc}(\pi Yv)\right|^2,\tag{2.128}$$

where $NPS_{OD}(u, v)$ is the NPS of $OD(x, y)$, and therefore,

$$NPS_d(0,0) = NPS_{OD}(0,0).\tag{2.129}$$

If both dimensions of the measurement area X and Y are large with respect to any correlation distance in $OD(x, y)$, $NPS_{OD}(u, v)$ can be approximated as a constant value for all frequencies at which the sinc functions have a non-negligible value. The variance in $d(x, y)$ can then be written as

$$\sigma_d^2 = \int_{-\infty}^{\infty} NPS_d(u,v)\,du\,dv\tag{2.130}$$

$$\approx NPS_{OD}(0,0)\int_{-\infty}^{\infty}\left|\text{sinc}(\pi Xu)\text{sinc}(\pi Yv)\right|^2\,du\,dv\tag{2.131}$$

$$= NPS_d(0,0)\frac{1}{XY},\tag{2.132}$$

and therefore

$$\text{NPS}_d(0, 0) \approx A\sigma_d^2, \tag{2.133}$$

where $A = XY$ is the measurement area. Equation (2.133) is in the form expressed on page 222 of Dainty and Shaw [5]. It shows that for this special case where measurements are made with an aperture (the sampling function) that is large relative to any correlation distance in the quantity being measured, the zero-frequency value is approximately equal to the measured variance multiplied by the measurement area.

This result may be useful when an accurate measure of the zero-frequency value is required. In practice, if Eq. (2.114) is used to calculate the NPS, a zero-frequency value of zero (or some other erroneous value) may be obtained when the sample mean is used as an estimate of the expectation value. It is important to note that the zero-frequency value is generally non-zero, and that its value can be affected by the measurement process. See the next section and Eq. (2.252) for additional specific implications of the zero-frequency value.

2.6.2.3 NPS, autocovariance and variance of a distribution of uncorrelated quanta

An uncorrelated two-dimensional distribution of image quanta $q(x, y)$, such as a uniform distribution of x rays, has an NPS given by [5]

$$\text{NPS}_q(u, v) = \text{E}\{q(x, y)\} = \text{E}\{q\}, \tag{2.134}$$

which is equal to $\text{E}\{q\}$, the expected number of quanta per mm^2, and is independent of spatial frequency. Note that the units of the NPS of a quantum image are different from that of an analog or digital image (which are mm^2, see Section 2.2.1). This is because quantum images are distributions, requiring distribution theory for interpretation, while analog images and digital images are not.

The corresponding autocovariance is given by

$$K_q(x, y) = \text{E}\{\Delta q(x', y')\Delta q(x' + x, y' + y)\} \tag{2.135}$$

$$= \begin{cases} \text{E}\{|\Delta q(x, y)|^2\} & \text{for } x = 0, \ y = 0 \\ 0 & \text{for } x \neq 0, \ y \neq 0 \end{cases} \tag{2.136}$$

$$= \text{E}\{q\}\delta(x, y), \tag{2.137}$$

which is a δ function scaled by $\text{E}\{q\}$. The fact that the autocovariance is proportional to a δ function is equivalent to stating that the image quanta are uncorrelated. That is, there is no statistical correlation of quanta at any position x, y with any other position x', y'.

For this special case of a distribution of uncorrelated quanta, the zero-frequency value of the NPS is obtained by combining Eqs. (2.122) and (2.137), giving

$$\text{NPS}_q(u, v)|_{u,v=0,0} = \int_{-\infty}^{\infty} \int_{-\infty}^{\infty} \text{K}_q(u, v) \, du \, dv \qquad (2.138)$$

$$= \int_{-\infty}^{\infty} \int_{-\infty}^{\infty} \text{E}\{q\}\delta(x, y) \, du \, dv \qquad (2.139)$$

$$= \text{E}\{q\}. \qquad (2.140)$$

The variance of this distribution of image quanta, given by

$$\sigma_q^2 = \int_{-\infty}^{\infty} \int_{-\infty}^{\infty} \text{NPS}_q(u, v) \, du \, dv = \int_{-\infty}^{\infty} \int_{-\infty}^{\infty} \text{E}\{q\} \, du \, dv, \qquad (2.141)$$

is undefined.

In practice, a uniform distribution of x rays coming from a medical x-ray tube will be uncorrelated and as a result have a flat NPS as given by Eq. (2.134) [5]. However, it should be noted that while a distribution of secondary quanta (such as light from a radiographic screen) will always have an uncorrelated component, they may also be partially correlated. Thus, the NPS of a distribution of secondary quanta may not be flat but will always have a non-zero component extending to essentially infinite frequencies.

2.6.3 Noise-equivalent number of quanta (NEQ)

As indicated above, units of the NPS depend on the physical basis of the image signal $d(x)$ and may be arbitrary or specific to a particular imaging system. Thus, use of the NPS for quantifying image noise brought the practical problem of absolute scaling of signal and noise-power spectra. By expressing image noise in terms of the number of Poisson-distributed input photons per unit area at each spatial frequency, Shaw obtained a common *absolute* scale of noise—the noise-equivalent number of quanta (NEQ) [5, 30]. The NEQ of a linear system can be defined as

$$\text{NEQ}(\bar{q}, u) = \frac{|\bar{q} \, \text{T}(u)|^2}{\text{NPS}(u)}, \qquad (2.142)$$

for an average input of $\bar{q}$ quanta per unit area where $\text{T}(u)$ is the system characteristic function describing signal transfer from input to output of an imaging system (Section 2.3.2.2). The numerator describes the (squared) expected output signal in terms of the spatial-frequency response of the system, $|\bar{q} \, \text{T}(u)|^2$. The denominator describes the corresponding output noise power. In general, if the average output signal from a linear system is $\bar{d}$, corresponding to an average uniform input of $\bar{q}$ quanta per unit area, the system large-area gain factor is $G = \bar{d}/\bar{q}$ and

$|T(u)| = G\,\mathrm{MTF}(u)$. Therefore,

$$\mathrm{NEQ}(\bar{q}, u) = \frac{\bar{q}^2 \bar{G}^2 \mathrm{MTF}^2(u)}{\mathrm{NPS}_d(u)} \qquad (2.143)$$

$$= \frac{\mathrm{MTF}^2(u)}{\mathrm{NPS}_d(u)/\bar{d}^2}, \qquad (2.144)$$

where $\mathrm{NPS}_d(u)$ is the output image NPS. The units of NEQ are equal to those of $\bar{q}$.

Equation (2.144) is particularly convenient to use in many practical situations as it only requires $\mathrm{MTF}^2(u)$ and the NPS normalized by the mean signal squared, $\mathrm{NPS}_d(u)/\bar{d}^2$, both of which are readily determined experimentally from measured image data.

Some systems have a nonlinear response and exhibit only small-signal linearity. A more general form of the NEQ that is still valid for these systems can be written as [28]

$$\mathrm{NEQ}(\bar{q}, u) = \frac{\bar{q}^2 \left|\dfrac{\partial \bar{d}}{\partial \bar{q}}\right|^2 \mathrm{MTF}^2(u)}{\mathrm{NPS}_d(u)}, \qquad (2.145)$$

where $\partial \bar{d}/\partial \bar{q}$ is the incremental change in average output signal $\bar{d}$ attributable to an incremental change in the average input signal $\bar{q}$ at an average input level $\bar{q}$. For example, film-screen systems have a nonlinear response to x-ray exposure. Using Eq. (2.145), the NEQ for these systems can be written as [5]

$$\mathrm{NEQ}(\bar{q}, u) = \frac{\bar{q}^2 |\gamma \log_{10}(e)(1/\bar{q})|^2 \mathrm{MTF}^2(u)}{\mathrm{NPS}_{OD}(u)} \qquad (2.146)$$

$$= \frac{(\gamma \log_{10} e)^2 \mathrm{MTF}^2(u)}{\mathrm{NPS}_{OD}(u)}, \qquad (2.147)$$

where γ is the slope of the characteristic optical density versus log-exposure curve (and therefore the system gain factor is $\bar{G} = \gamma \log_{10}(e)(1/\bar{q})$) corresponding to the same exposure level (and therefore mean optical density, $\overline{OD}$) as the optical-density NPS measurement, and the MTF corresponds to a small-signal MTF.

The NEQ concept expresses image quality on an absolute scale, independent of specific system parameters. It gives the number of Poisson-distributed quanta that would produce the same SNR given an ideal detector. It can be measured for specific systems at specified exposure levels in various laboratories, and the results can be directly compared. An image with a greater NEQ corresponds to lower image noise. An ideal system that transfers both signal and noise with only a scaler gain factor G results in an NEQ given by

$$\text{NEQ}(\bar{q}, u) = \frac{|\bar{q}G|^2}{G^2\bar{q}} = \bar{q}, \tag{2.148}$$

which has no frequency dependence and is the best possible NEQ for an input $\bar{q}$.

Interpretation of the NEQ often requires considerable thought, but provides a great deal of insight regarding the information content of an image. It is a measure of the density of quanta the image is "worth" [31]. Wagner and co-workers [31–34] have shown that the NEQ concept can be generalized to other imaging modalities including computed tomography (CT), magnetic resonance imaging (MRI), and ultrasound imaging. They introduced the concept of a "system aperture," a_{ap}, and showed that it is related to the NEQ through the equation

$$a_{ap}^{-1} = \int_{-\infty}^{\infty} \frac{\text{NEQ}(k)}{\text{NEQ}(0)} \, d^2k. \tag{2.149}$$

The system aperture is the fundamental measure of resolution in a noise-limited imaging system [31]. They also showed that for the detection of an object $\Delta s(x)$ having frequency components $\Delta S(u)$, the NEQ is directly related to the "ideal observer SNR," SNR_i, according to

$$\text{SNR}_i^2 = \int_{-\infty}^{\infty} |\Delta S(u)|^2 \text{NEQ}(u) \, du. \tag{2.150}$$

The ideal observer detects all of the information in the image for the required task, and SNR_i determines the performance of the observer in detection tasks.

Decision-making theory is a complex subject. A summary of important aspects of image quality, observer performance and detection theory, including the NEQ, is available as an ICRU report [28] "Medical imaging—the assessment of image quality" written by some of the most important figures in this field, including Barber, Brown, Burgess, Metz, Myers, Taylor, and Wagner.

2.6.4 Detective quantum efficiency (DQE)

The NEQ describes the effective number of Poisson-distributed x-ray quanta contributing to image SNR. Using a similar approach, the detective quantum efficiency (DQE) is a measure of the effective *fraction* of incident Poisson-distributed quanta contributing to image SNR. Thus, the NEQ is a measure of image quality while the DQE is a similar measure of system performance. The spatial-frequency-dependent DQE was first used during the mid-seventies in an attempt to develop measures of system performance common to a variety of imaging technologies by Shaw, Wagner, and co-workers [35, 36], with Wagner and co-workers [28, 36] deserving much of the credit for championing the widespread application of the noise-equivalent approach and providing some of the first absolute sets of DQE measurements. The DQE is defined as [30]

$$\text{DQE}(\bar{q}, u) = \frac{\text{NEQ}(\bar{q}, u)}{\bar{q}} \tag{2.151}$$

$$\equiv \frac{\overline{q}\left|\dfrac{\partial \overline{d}}{\partial \overline{q}}\right|^2 \mathrm{MTF}^2(u)}{\mathrm{NPS}_d(u)}.$$

(2.152)

A practical expression for use when measuring the DQE of a linear system is given by

$$\mathrm{DQE}(\overline{q}, u) = \frac{\overline{q}\,\overline{G}^2 \mathrm{MTF}^2(u)}{\mathrm{NPS}_d(u)}$$

(2.153)

$$= \frac{\overline{d}^2 \mathrm{MTF}^2(u)}{\overline{q}\,\mathrm{NPS}_d(u)}.$$

(2.154)

In the absence of additive system noise or multiplicative noise such as fixed-pattern noise, the DQE is independent of $\overline{q}$ and $\mathrm{DQE}(\overline{q}, u) = \mathrm{DQE}(u)$ for a linear imaging system. The DQE also depends on $\overline{q}$ for nonlinear systems such as film-screen systems. The DQE is always dimensionless, and can have a value no greater than unity.

The term $\overline{q}$ in Eq. (2.154) is normally interpreted as the total number of incident quanta per unit area, independent of energy of the quanta. It can be estimated from a measurement of the actual exposure X at the detector input (excluding backscatter) with the expression

$$\overline{q} = X\left(\frac{\Phi}{X}\right),$$

(2.155)

where X is the measured exposure (in roentgens), and (Φ/X) is the x ray fluence per R for the particular spectrum used. X-ray tube manufacturers may provide this factor for particular test conditions. Alternatively, if the incident spectrum $\Phi(E)$ (quanta mm^{-2} keV^{-1}) can be either measured or calculated, (Φ/X) can be estimated for that spectrum as

$$\left(\frac{\Phi}{X}\right) = \int_0^{kVp} \Phi_{rel}(E)\left[\frac{\Phi}{X}(E)\right] dE,$$

(2.156)

where $\Phi_{rel}(E)$ is the normalized incident x-ray spectrum, and $(\Phi/X)(E)$ is the fluence per unit exposure for a mono-energetic beam with energy E and is given by [37]

$$\frac{\Phi}{X}(E) = \frac{WQ}{\left(\dfrac{\mu_{en}(E)}{\rho}\right)_{air} Ee10^8},$$

(2.157)

where $(\mu_{en}/\rho)_{air}$ is the mass energy absorption coefficient (cm^2/g) for air, E is the x-ray energy (keV), e is the electronic charge (1.6022×10^{-19} Coul), W is
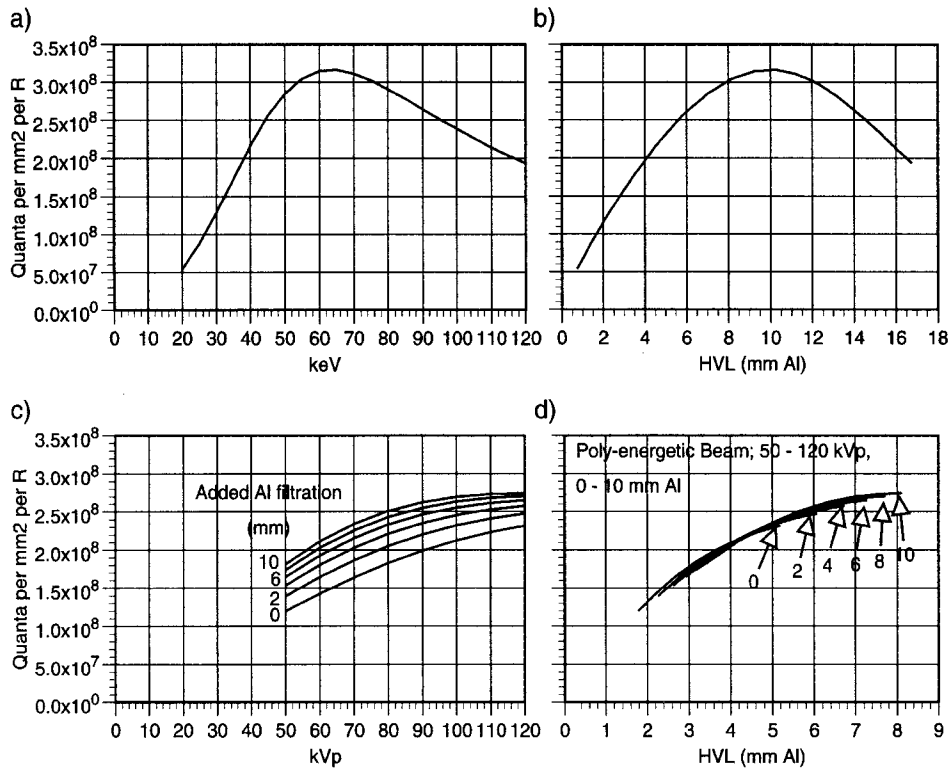
Figure 2.20: The conversion factor Φ/X (quanta mm^{-2} R^{-1}) is shown: a) as a function of mono-energetic keV; b) as a function of beam HVL for a mono-energetic beam; c) as a function of kVp for a poly-energetic beam with various thicknesses of added aluminum; and d) as a function of HVL for the same poly-energetic beams with added aluminum.

the work function of air (33.97 eV), and Q is the charge liberated in air by one Roentgen (exactly 2.580×10^{-4} $Coul\,kg^{-1}\,R^{-1}$). Values of (Φ/X) obtained with Eq. (2.157) are shown in Figure 2.20(a) for mono-energetic beams with energies between 20 and 120 keV, and in Figure 2.20(b) as a function of half-value layer (HVL) in mm of Al for the same beams.

Knowing an actual spectrum accurately is difficult or impractical in most situations. However, spectra can be calculated theoretically for specific situations and used to estimate (Φ/X) as a function of kVp. Figure 2.20(c) shows values of (Φ/X) calculated using Eq. (2.157) for various thicknesses of added aluminum and spectra generated using the method of Tucker [38]. It is clear that the actual value of (Φ/X) is specific to details of the spectrum used, but *insensitive* to both kVp and thickness of added aluminum when expressed as a function of the beam HVL as shown in Figure 2.20(d). Thus, an estimate of (Φ/X) with sufficient accuracy can often be obtained using Figure 2.20(d) if the HVL can be measured for the particular test conditions.

The DQE is sometimes written as

$$DQE(u) = \frac{SNR_{out}^2(u)}{SNR_{in}^2(u)},$$ (2.158)

although this form must be used with caution. It is only correct if the squared output SNR is given by $SNR_{out}^2(u) = \bar{d}^2 MTF^2(u)/NPS_d(u)$ and the squared input SNR by $SNR_{in}^2(u) = SNR_{ideal}^2(u) = \bar{q}$ where $SNR_{ideal}^2(u)$ corresponds to a photon-counting detector rather than any other type of detector such as an energy-integrating detector. Equation (2.152) should be taken as the general definition of the DQE.

2.7 Noise transfer in cascaded imaging systems

As discussed in the previous section, image quality is directly tied to the number of image quanta interacting with the imaging system. However, there may be additional factors degrading image quality if the imaging system is not optimally designed. For instance, when input quanta are converted to secondary quanta, such as the conversion of interacting x rays into optical quanta in a scintillating phosphor, image quality may also be influenced by the number of secondary quanta. One way of understanding the effect of these conversions is to represent the system as a "cascade" of multiple processes, and use *transfer theory* to describe the transfer of signals and noise through the system.

In addition to understanding the different approaches available for specifying system performance as described in the previous section, it is often necessary to determine whether a particular imaging system is performing at a level close to what can be expected for a particular design. In this section, methods are described which can be used to predict system performance based on design parameters. The approach is based on *transfer theory*, in which a system is modeled as a serial cascade of many stages. Transfer of signal and noise through the entire system is predicted from an understanding of the transfer properties of each stage.

In many systems, input x-ray quanta are converted to other forms of energy before producing a final image. For instance, x rays may be converted to light quanta in a radiographic screen, which may subsequently be converted to electron-hole carrier pairs in a detector. In an image intensifier, x rays are converted to light and then to photo-electrons which are accelerated before being converted to light again in the output phosphor. In some cases, the number of quanta transferred through each stage, as well as statistical correlations introduced into the distributions of these quanta, play critical roles in determining the final image quality. For instance, an inadequate number of quanta may result in a secondary "quantum sink" (see below) which will degrade image quality. In this section, methods of representing a complex system as a cascade of elementary stages are described. Transfer relationships are given for the transfer of signal and noise through these stages, and can be combined to predict the overall system DQE.

There are three elementary processes that play an important role in understanding noise transfer: (a) quantum amplification; (b) deterministic blurring; and, (c) quantum scattering. They can be cascaded in appropriate serial combinations where the output of one stage forms a virtual input to the next. Many systems of practical importance can be modeled, and overall system signal-and-noise transfer determined to a good approximation. In most cases, the input and output of each stage is a distribution of quanta. These quanta may be of any form, including x rays, light, and other forms, as long as they can be considered to be independent of each other. The input and output may even represent the spatial distribution of some type of event, such as interacting quanta or just photo-electric interactions. In the following section, noise-transfer characteristics through each elementary process and methods of cascading multiple stages to predict system performance are described.

2.7.1 Quantum amplification

The first elementary process represents a conversion of quanta from one form to another, such as the conversion of x-ray quanta to optical quanta in a radiographic screen. Both the input and output of this stage are quantum images (Section 2.2.1.3). Each input quantum is converted to $\tilde{g}$ output quanta where $\tilde{g}$ is a random variable characterized in terms of a mean gain factor, $\bar{g}$, and variance, σ_g^2. Thus, if $q_{in}(r)$ is a sample function describing a sample distribution of input quanta,

$$q_{out}(r) = \tilde{g}q_{in}(r).\tag{2.159}$$

Rabbani, Shaw and Van Metter [39] showed that the mean number of quanta in a quantum image passing through this amplification stage is transferred according to

$$\bar{q}_{out} = \bar{g}\,\bar{q}_{in},\tag{2.160}$$

where $\bar{q}_{in}$ is the expected number of quanta per unit area in the input and $\bar{q}_{out}$ is the expected number in the output. They also showed that the NPS is transferred according to

$$\text{NPS}_{out}(k) = \bar{g}^2\text{NPS}_{in}(k) + \bar{q}_{in}\sigma_g^2.\tag{2.161}$$

These expressions can be used to describe the transfer of a uniform distribution of image quanta through an amplification process as represented graphically in Figure 2.21, and can be combined with signal-and-noise transfer expressions for other elementary processes described below to predict the performance of complex systems.

$q_{in}(r)$

$NPS_{in}(k)$

$\overline{g}, \sigma_g^2$

$q_{out}(r)$

$NPS_{out}(k)$
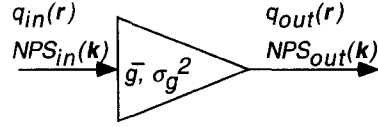
Quantum Amplification or Selection

Figure 2.21: The process of quantum amplification (and binomial selection) is represented as shown here, characterized by a mean gain $\overline{g}$ and variance σ_g^2.

2.7.1.1 Binomial selection

The amplification stage described above can also be used to represent a binomial selection process, such as the quantum efficiency of a detector. This is a special case of the amplification process in which $\widetilde{g}$ is a random variable that can have a value of 1 or 0 only. That is, each quantum incident on this selection stage is either transferred (probability $\overline{g}$), or not (probability $1 - \overline{g}$), to the output where the average value $\overline{g}$ is the quantum efficiency of the process. As a consequence of the binomial theorem, the variance σ_g^2 becomes [17]

$$\sigma_g^2 = \overline{g}(1 - \overline{g}). \tag{2.162}$$

Noise transfer through a quantum selection process is therefore given by

$$NPS_{out}(k) = \overline{g}^2 NPS_{in}(k) + \overline{q}_{in}\overline{g}(1 - \overline{g}) \tag{2.163}$$

$$= \overline{g}^2 [NPS_{in}(k) - \overline{q}_{in}] + \overline{q}_{in}\overline{g}. \tag{2.164}$$

The component $NPS_{in}(k) - \overline{q}_{in}$ is called the *correlated noise* component, and $\overline{q}_{in}$ is called the *uncorrelated noise* component. As shown by Eq. (2.164), it is sometimes said that the correlated component is "passed through" the squared conversion gain $\overline{g}^2$ in keeping with the ideal of a transfer model, while the uncorrelated component is passed though $\overline{g}$. A significant correlated component occurs when $NPS_{in}(k) \ll \overline{q}_{in}$. When the input quanta are uncorrelated, in other words, randomly distributed, then $NPS_{in}(k) = \overline{q}_{in}$. This corresponds to the smallest value that $NPS_{in}(k)$ can have, and results in an output NPS given by

$$NPS_{out}(k) = \overline{q}_{in}\overline{g}, \tag{2.165}$$

which is the expected result.

2.7.2 Deterministic blur

The second elementary process is called deterministic blurring (Figure 3.22), describing situations where image blur is accurately expressed as a convolution of
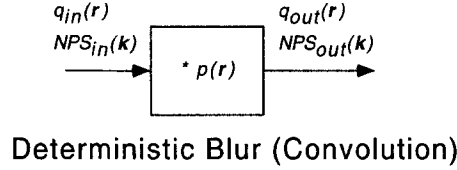
Deterministic Blur (Convolution)

Figure 2.22: Deterministic blur is represented as a convolution (linear filter). It occurs when the input signal is redistributed with a *weighting* given by the PSF.

the input with a point-spread function. The input can be either a quantum image $q(r)$ or an analog signal, but the output can only be an analog signal $d(x)$ where

$$d(r) = q(r) * \mathrm{psf}(r),\tag{2.166}$$

and $\mathrm{psf}(r)$ is the blur PSF. When the PSF is normalized to unity area,

$$\overline{d}_{out} = \overline{q}_{in},\tag{2.167}$$

and

$$\mathrm{NPS}_{out}(k) = \mathrm{NPS}_{in}(k)\mathrm{MTF}^2(k),\tag{2.168}$$

where $\mathrm{psf}(r)$ and $\mathrm{MTF}(k)$ are the PSF and MTF describing the weighting of the blur. Thus, the NPS is passed through the squared MTF. An example of deterministic blur is given later in the description of the integration of image quanta in a digital detector element (Section 2.9.1).

2.7.3 Quantum scatter

Most image-blurring mechanisms, including blur caused by the scattering of optical quanta in a radiographic screen, are fundamentally scattering processes. That is, each quantum is randomly relocated to a new location with a probability described by the normalized PSF of the blur (Figure 2.23). This differs from deterministic blur which can be viewed as a redistribution of signal by weights (as described by the convolution integral), while scatter must be viewed as a redistribution by probabilities. This distinction has been recognized for some time (e.g., Dainty and Shaw [5], Wagner [32], Metz [12], Sandrik and Wagner [34], Metz and Vyborny [40], and Barrett and Swindell [13]). It was first expressed by Shaw and Van Metter [19], derived theoretically by Rabbani, Shaw and Van Metter [39], and derived again more recently using point-process theory by Barrett [41].

The output of a scatter stage must necessarily be a sample quantum image and can be written as

$$q_{out}(r) = q_{in}(r) *_s \mathrm{psf}(r),\tag{2.169}$$

Quantum Scatter
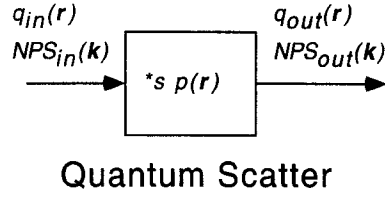
Figure 2.23: Scatter was described by Rabbani *et al.* [39] and occurs when individual quanta are redistributed with a *probability* given by the normalized PSF. It is represented as a scatter operator in this transfer-theory formalism.
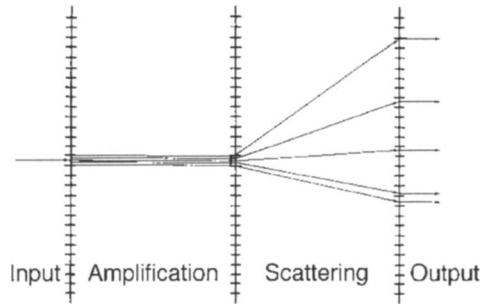
Figure 2.24: Quantum amplification and scatter operators are cascaded to describe processes involving image quanta. An amplification stage followed by a scattering stage as illustrated here is used to represent the conversion of x rays to light in a radiographic screen.

where psf(r) is the scatter PSF normalized to unity area and $*_s$ represents a scatter operator [42]. Rabbani *et al.* [39] showed that $\overline{q}$ and NPS(k) are transferred through a scatter process according to

$$\overline{q}_{out} = \overline{q}_{in}, \tag{2.170}$$

and

$$\text{NPS}_{out}(k) = \left[\text{NPS}_{in}(k) - \overline{q}_{in}\right]\text{MTF}^2(k) + \overline{q}_{in}, \tag{2.171}$$

where psf(x) and MTF(k) are the PSF and MTF describing the scattering probabilities normalized to unity area.

It is worth noting other differences (and similarities) between deterministic blur (Eq. (2.168)) and quantum scatter (Eq. (2.171)). For instance, deterministic blur will always pass the NPS through the squared MTF. This blur corresponds to the linear filter described in many standard texts on linear systems and Fourier transforms. Scatter is a stochastic translated point process and will pass the correlated component of the NPS through the squared MTF, resulting in a frequency-dependent noise term. The frequency-independent term corresponds to the uncorrelated noise component, and is not passed through the MTF [39]. Other properties

of this scatter operator, which has also been called a "stochastic convolution," are described elsewhere [42].

The three elementary processes, amplification, convolution, and scatter, can be cascaded to represent a wide variety of physical process. Of particular importance is the simple cascade of an amplification stage followed by a scattering stage as illustrated in Figure 2.24. This combination can be used to represent the conversion of x rays into light in a radiographic screen, including the scatter of light within the screen.

2.8 Cascaded DQE and quantum sinks

2.8.1 Particle-based approach

Noise transfer through a cascaded system was first examined for the analysis of cascaded multi-stage photo-multiplier detectors by Shockley and Pierce [43]. In particular, Zwieg [25] showed that the DQE of a system consisting of M Poisson gain stages is given by

$$\text{DQE}(u) = \cfrac{1}{1 + \cfrac{1}{\bar{g}_1} + \cfrac{1}{\bar{g}_1\bar{g}_2} + \cdots + \cfrac{1}{\bar{g}_1\cdots\bar{g}_M}} \tag{2.172}$$

$$= \cfrac{1}{1 + \cfrac{1}{P_1} + \cfrac{1}{P_2} + \cdots + \cfrac{1}{P_M}}, \tag{2.173}$$

where P_j is the product of the gains for all stages preceding and including the jth stage:

$$P_j = \prod_{i=1}^{j} \bar{g}_i. \tag{2.174}$$

Equation (2.173) is particularly useful. It shows that the system DQE is degraded if the value of P_j for any stage is less than approximately one. P_j gives the number of quanta at the jth stage normalized to the number of input quanta and, if this number is less than one, the system is said to have a "quantum sink" at that stage. In this type of analysis, the first factor P_1 is generally the quantum efficiency of the detector, which is always less than unity. This is sometimes called the primary quantum sink. It is particularly important during the design of any system to ensure that an adequate number of quanta will exist at each subsequent stage to avoid any secondary quantum sinks. In general, Eq. (2.173) suggests that a secondary quantum sink would be avoided so long as the condition

$$P_j > 10, \tag{2.175}$$
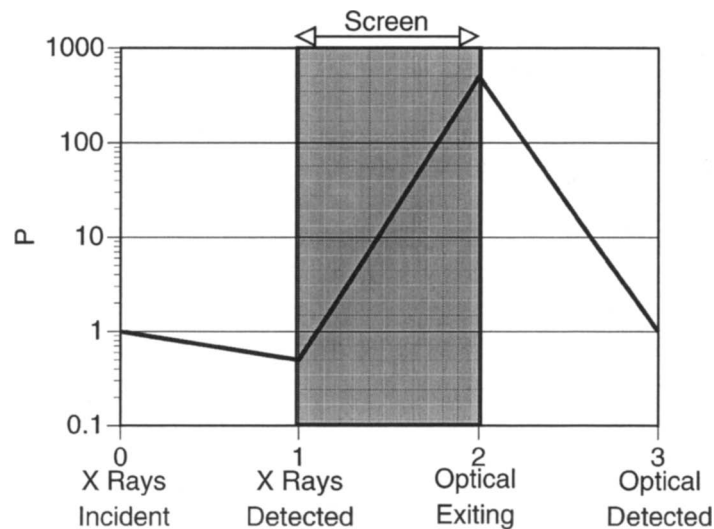
Figure 2.25: Particle-based QAD analysis showing P_j as a function of stage number j.

is satisfied. However, as shown in the next section, this condition is not restrictive enough to be useful in practice.

This simple quantum-sink analysis can be performed for an imaging system based on design parameters by representing the system as a simple cascade of amplification stages. The factors P_j can be illustrated graphically as a function of the stage number j as illustrated in Figure 2.25, clearly showing the existence of a quantum sink if any of the factors is less than, or close to, unity. It is often the first step in assessing the potential of any system design for producing high-quality images [44–48].

This type of analysis in imaging can be traced directly to Albert Rose in the nineteen-forties. He published what is thought to be the first analysis of this type in which he assessed a video chain using a model that included the television pickup tube and lenses, video amplifiers and CRT display, and the retina in an observer. He plotted the number of image quanta at each stage and showed that two quantum sinks were predicted: one at the photo cathode of the pickup tube and the other at the photo surface of the retina [3].

This approach is useful for "back-of-the-envelope"-type calculations of the DQE. However, it is now known to be overly simplistic and responsible for much wasted effort in the development of some new designs because of its failure to predict quantum sinks at non-zero spatial frequencies. Even today, Eq. (2.173) is sometimes used to predict a high DQE for system designs that have no chance of success. For this reason, it is labeled as a "particle approach," and must be interpreted with caution.

2.8.2 Fourier-based Approach

The particle-based Zwieg-type model was generalized to include second-order statistics by Cunningham *et al.* [49] using the noise-transfer relationships of Rabbani *et al.* [39]. They showed that the frequency-dependent DQE of a cascaded system consisting of M amplification and scattering stages is described by

$$
\text{DQE}(u) = \cfrac{1}{1 + \cfrac{1 + \varepsilon_{g_1}\text{MTF}_1^2(u)}{\bar{g}_1\text{MTF}_1^2(u)} + \cdots + \cfrac{1 + \varepsilon_{g_M}\text{MTF}_M^2(u)}{\bar{g}_1 \ldots \bar{g}_M \text{MTF}_1^2(u) \ldots \text{MTF}_M^2(u)}}, \quad (2.176)
$$

where ε_{g_j} is called the amplification Poisson excess of the jth stage given by

$$
\varepsilon_{g_j} = \frac{\sigma_{g_j}^2}{\bar{g}_j} - 1. \quad (2.177)
$$

The amplification Poisson excess is the relative amount by which the variance exceeds that of Poisson amplification. Poisson amplification corresponds to a variance $\sigma_{g_j}^2 = \bar{g}_j$ and excess $\varepsilon_{g_j} = 0$. Deterministic gain (a gain with no random variability) corresponds to a variance $\sigma_{g_j}^2 = 0$ and excess $\varepsilon_{g_j} = -1$. $\text{MTF}_j(u)$ is the MTF resulting from the scattering process at the jth stage. Each stage can represent only an amplification or scattering process, but not both. For amplification at the jth stage, $\text{MTF}_j(u) = 1$. For a scattering jth stage, $\bar{g}_j = 1$ and $\varepsilon_{g_j} = -1$.

In practice, the excess terms are often small enough to be neglected and Eq. (2.176) then simplifies to

$$
\text{DQE}(u) \approx \cfrac{1}{1 + \cfrac{1}{\bar{g}_1\text{MTF}_1^2(u)} + \cdots + \cfrac{1}{\bar{g}_1 \ldots \bar{g}_M\text{MTF}_1^2(u) \ldots \text{MTF}_M^2(u)}} \quad (2.178)
$$

$$
= \cfrac{1}{1 + \cfrac{1}{P_1(u)} + \cdots + \cfrac{1}{P_M(u)}}, \quad (2.179)
$$

where $P_j(u)$ is the product of all gains and squared MTF's for all stages preceding and including the jth stage:

$$
P_j(u) = \prod_{i=1}^{j} \bar{g}_i\text{MTF}_i^2(u). \quad (2.180)
$$

The Fourier-based Eq. (2.179) has a pleasing symmetry with the particle-based Eq. (2.173), although it differs in an important respect. It shows that scattering

stages degrade the DQE dramatically when the MTF value drops with increasing spatial frequency. The simpler particle-based analysis may not predict a secondary quantum sink when in fact image quality is being degraded for that reason at non-zero spatial frequencies.

Additive noise may, in principle, be added to the image by components in the imaging chain. This source of noise is ignored here for simplicity, but can be incorporated into an estimate of the DQE if necessary [49]. In addition, it should be noted that for systems that may incorporate geometric magnification or demagnification of the image (such as with an image-intensifier based system), $\bar{q}$ and NPS(u) must be expressed relative to a fixed plane of reference. For convenience, that plane of reference is often the input surface of the detector.

2.8.3 General criteria to avoid a secondary quantum sink

A general criteria can be developed to ensure that a secondary quantum sink does not degrade the DQE for any frequency of interest. If the maximum frequency of interest u_{max} is taken as the maximum frequency passed corresponding to $\text{MTF}(u_{max}) \approx 0.33$, then $\text{MTF}^2(u_{max}) \approx 0.1$ and the following statement applies:

A secondary quantum sink can be avoided if the condition $P_j(u) > 10$ is satisfied at each stage in a cascaded system for all spatial frequencies of interest. This can generally be achieved if all quantum amplification factors subsequent to the primary selection stage are sufficiently large to ensure that

$$P_j(0) > 100. \tag{2.181}$$

Specific values will depend on system particulars, but it is clear that the frequency dependence of this type of analysis results in a much more stringent condition as given by Eq. (2.181) than that predicted by the simpler particle approach given by Eq. (2.175).

2.8.4 Quantum accounting diagrams (QAD)

The significance of $P_j(u)$ is so great in an analysis of system performance that it is informative to plot $P_j(u)$ as a function of stage number j for any spatial frequency of interest. These graphs have been called "quantum accounting diagrams" (QADs) [49]. They illustrate an "effective number of quanta" (not to be confused with the noise-equivalent number of quanta, NEQ [5, 28, 32]) at each stage of the system as a function of spatial frequency.

The QAD for the hypothetical system (assuming typical values for the various parameters) is shown in Figure 2.26. The abscissa is the stage number, j, for $j = 0 \ldots M$ (stage 0 corresponds to the x rays incident on stage 1). The ordinate is the value of $P_j(u)$. Multiple lines are drawn indicating multiple spatial frequencies of
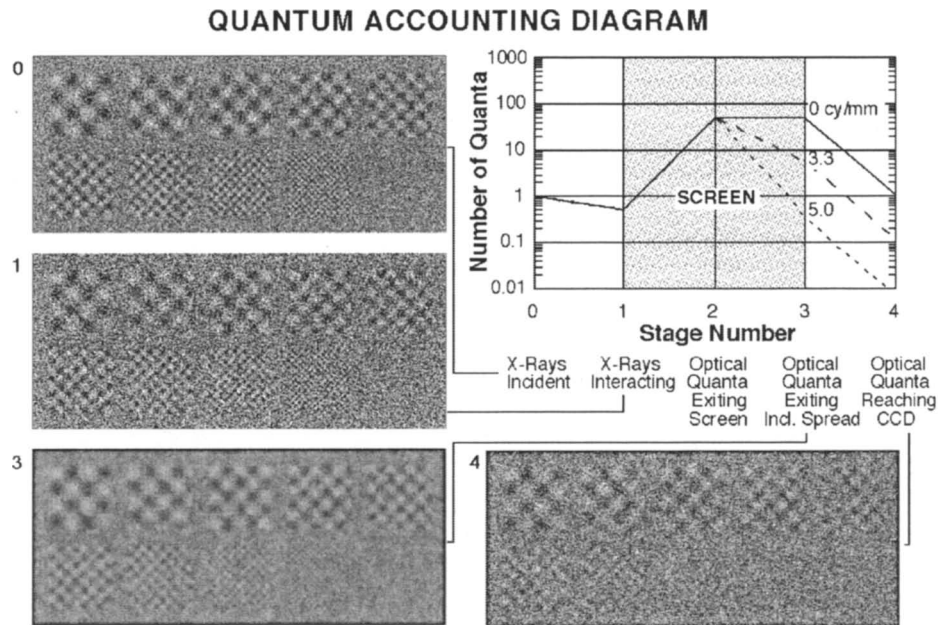
QUANTUM ACCOUNTING DIAGRAM

Figure 2.26: Quantum Accounting Diagram of the hypothetical system and simulated images using a Monte Carlo calculation illustrating the visual impact of the non-zero spatial-frequency quantum sink.

interest. The lines all start at $P_0(u) = 1$, corresponding to a single incident x-ray quantum.

The first step is detection of the incident x rays to select those x rays which interact assuming a quantum efficiency $\alpha = 0.5$. The QAD lines for all frequencies therefore decrease from 1.0 to 0.5.

This is followed by conversion of the interacting x rays to optical quanta, assuming a conversion factor $\bar{g} = 1000$. This value is of course x-ray energy dependent. Therefore, the value chosen is the appropriate average for the actual spectrum of *interacting* (not incident) x rays.

The third stage describes the spatial spreading of light in the screen attributable to geometric considerations and scattering. Details of what causes the spread are unimportant as long as the MTF of the blur is known, and all optical quanta are independent. The lines corresponding to each spatial frequency diverge as each line is decreased to a new value according to the square of the MTF (for that stage) at each frequency. Thus, at a frequency corresponding to $MTF_r(u) = 0.1$, the QAD value is reduced by a factor of 0.01 while the QAD value at $u = 0$ is not decreased at all. This separation of the various frequency lines may cause a large decrease in the DQE at high spatial frequencies, with little or none at low spatial frequencies.

The final stage in the model is selection of those optical quanta that escape from the screen and are coupled from the screen to the detector by the lens as-

sembly, and are detected by the imaging detector. It may be noted that this process could also be reasonably represented as several individual selection stages, corresponding to escape from the screen, collection by the lens (solid angle considerations), transmission through the lens, detection by the detector, etc. However, it has been shown [42] that multiple selection stages can be combined into a single stage and, in fact, the relative order of selection and stochastic spreading stages can be reversed without affecting the resulting DQE. Thus, the physicist has some discretion in choosing how the system is to be represented. The coupling efficiency giving the probability that an optical quantum exiting from the screen is detected by the optical detector in the hypothetical system is $\beta = 0.02$.

Examination of Eq. (2.176) shows that if a single stage has a $P_j(u)$ value much less than both unity and all other stages, that value will effectively determine the DQE of the system. That limiting stage is sometimes called the dominant "quantum sink" because it is the stage with the fewest number of quanta. Figure 2.26 shows that for this system, the dominant quantum sink is frequency dependent. For example, when $u = 0$, there is not one single dominant quantum sink, but the system DQE will be determined largely by the number of x-ray quanta interacting in the screen (stage 1) with a minor additional degradation due to the number of optical quanta at stage 4. It is said that a minor secondary quantum sink exists in the number of optical quanta coupled to the detector. At higher spatial frequencies, the picture changes. For instance, when $u \approx 6.0$ cycles/mm or more, there is a dominant secondary quantum sink at stage 4.

The visual effect of quantum sinks in images is illustrated in Figure 2.26. A Monte Carlo study was performed [50] to simulate the images produced by a system with the QAD shown. Images are shown for each step in the cascaded model to illustrate how they are degraded while transferred through the system. The images contain 10 two-dimensional sinusoidal patterns with frequencies of 1.0, 1.1, 1.25, 1.4, 1.7, 2.0, 2.5, 3.3, 5.0, and 10.0 cycles/mm. Image 0 is an image composed of the quanta incident on the system, and represents the best possible image that could be produced with any system. Image 1 is composed of the detected quanta assuming a quantum efficiency of 0.5. The noise in this image has increased by a factor of the square root of two. Image 3 is composed of the optical quanta as they exit the screen. Spatial blurring of the light degrades the MTF, and the high-frequency patterns are harder to distinguish. Noise in this image has also been smoothed by the effect of optical blur. The large number of light quanta generated for each interacting x ray causes the stochastic blur to behave much like a deterministic blur. Image 4 is composed of the optical quanta that are coupled through a lens system to an optical detector. The light collection efficiency of the lens is not enough to avoid a secondary quantum sink at this stage for spatial frequencies above approximately 2.5 cycles/mm (as shown in the QAD). As a result, image noise masks patterns above this frequency, corresponding to a degraded DQE. The quantum sink also changes the appearance of noise in the image, which becomes more uniform for all spatial frequencies because of the frequency-independent term in Eq. (2.171). This represents the component of noise resulting from the uncorrelated optical quanta.

The secondary quantum sink makes this noise component dominant. Details of the appearance of the images depends on system parameters as well as the value chosen for $\bar{q}$; however, it is clear that image quality in this example is degraded because of the secondary quantum sink. This system also clearly fails the above condition expressed by Eq. (2.181) required to avoid a secondary quantum sink.

Image quality (at high frequencies) is therefore being compromised by an inadequate number of secondary quanta, and can only be improved by increasing the value of $P_4(u)$. This could be achieved by changing the screen to increase the number of optical quanta generated per interacting x ray (if that is possible without significantly degrading the screen MTF), or by increasing the optical collection efficiency by increasing the size (and therefore cost) of the lens assembly. See reference [50] for more simulated images illustrating the effect of quantum sinks.

The QAD analysis must be considered a "first approximation" to noise analysis, and reflects only the fundamental noise limitations imposed by Poisson statistics. It does not reflect noise limitations imposed by additive noise sources such as electronic amplifier noise. In addition, it will be noted that the gain variances do not appear in a calculation of the QAD. This is another reason why the QAD is a less accurate measure of image quality than an evaluation of the DQE with Eq. (2.176) which can include additive noise [49]. The utility of the QAD approach is that it is simple, visual, physically intuitive, and clearly identifies where quantum sinks may exist and what must be done to avoid them.

2.9 Metrics of digital-system performance

An analysis of noise in digital imaging systems is more complex, and the Fourier-based approach is almost always required. In this section, concepts of the digital MTF and digital NPS are introduced. These are then used to describe one way in which the NEQ and DQE of digital systems might be expressed.

A digital-imaging detector is viewed as a two-dimensional array of discrete detector elements. (Physical detector elements are called "dels" by Dr. Martin Yaffe to make a distinction from picture elements—"pixels"—as often they are not the same thing.) The detector produces a signal that is proportional to the number of quanta interacting in each detector element (Figure 2.27). Thus, each element functions as a spatial integrator of image quanta.

2.9.1 Detector-element size and the aperture MTF

Integration of quanta in each detector element can be represented as convolution with an aperture function in the spatial domain, giving rise to a corresponding "aperture MTF" in the spatial-frequency domain. This is illustrated in Figure 2.28, where a sample distribution of x-ray quanta $q(x)$ are incident on a detector. The left column shows $q(x)$ in one dimension, and the right column shows $|Q(u)|$ where $Q(u)$ is the Fourier transform of $q(x)$.

In the following it is assumed that each detector element has unity quantum efficiency and a width of a_x. The signal from the nth element centered at $x = nx_0$,
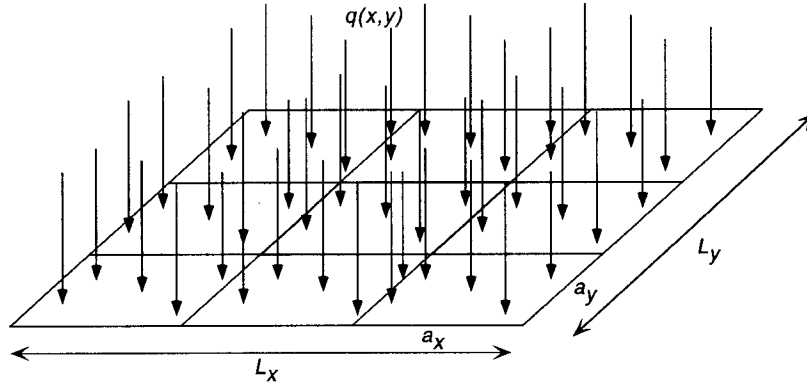
Figure 2.27: The detector array consists of an array of detector elements. Each element produces a signal proportional to the number of quanta interacting in the element.

d_n, is therefore given by the integral

$$d_n = k \int_{nx_0 - a_x/2}^{nx_0 + a_x/2} q(x) \, dx, \tag{2.182}$$

where k is a constant relating the number of interacting quanta to the detector output as a digital value. This integral can also be written as

$$d_n = k \int_{-\infty}^{\infty} q(x) \prod \left(\frac{x - nx_0}{a_x} \right) dx, \tag{2.183}$$

where

$$\prod \left(\frac{x}{a_x} \right) = \begin{cases} 1 & \text{for} \ -a_x/2 \leqslant x \leqslant a_x/2 \\ 0 & \text{otherwise.} \end{cases} \tag{2.184}$$

Equation (2.183) is recognized as being a correlation integral evaluated at the center of the element, $x = nx_0$, and hence

$$d_n = k \, q(x) \star \prod \left(\frac{x}{a_x} \right) \Bigg|_{x=nx_0}, \tag{2.185}$$

or similarly as the convolution of $q(x)$ with $\prod(-x/a_x)$,

$$d_n = k \, q(x) * \prod \left(\frac{-x}{a_x} \right) \Bigg|_{x=nx_0} = d(x)|_{x=nx_0}, \tag{2.186}$$

where

$$d(x) = kq(x) * \prod (-x/a_x). \tag{2.187}$$

Spatial Domain   Spatial-Frequency Domain
(magnitude)

a)

$q(x)$ $Q(u)$

b) $*k\,\Pi(x/a_x)$ $\times ka_x\,\mathrm{sinc}(\pi a_x u)$

a_x

$-1/a_x$ $1/a_x$

c) $= d(x)$ $= D(u)$

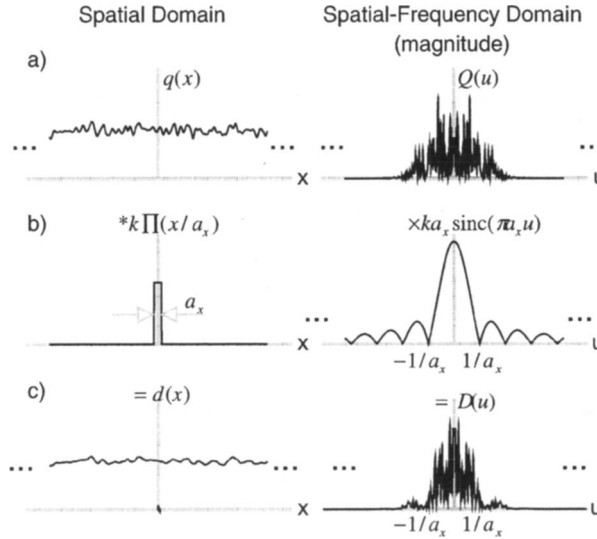$-1/a_x$ $1/a_x$

Figure 2.28: Integration of quanta in detector elements of width a_x is represented as convolution of $q(x)$ with $k\,\Pi(x/a_x)$ in the spatial domain, and multiplication with $ka_x\,\mathrm{sinc}(\pi a_x u)$ in the frequency domain.

The function $d(x)$ is called the *detector presampling signal*. It is a sample function that, when evaluated at positions corresponding to the center of each element, gives the detector output values for each element. Thus, $d(x)$ describes the detector signal for all possible detector-element positions, physical and non-physical.

This is a general result, showing that the effect of integrating quanta in a detector element can be represented as a convolution integral. The function $\Pi(-x/a_x)$ is the sampling function in the sense of distribution theory (Section 2.2.4), describing the measurement of $q(x)$. Convolution in the spatial domain corresponds to multiplication in the spatial-frequency domain, and Eq. (2.187) can therefore be expressed in the spatial-frequency domain as

$$D(u) = Q(u)\mathrm{T}_{a_x}(u),\qquad(2.188)$$

where $D(u)$ is the Fourier transform of $d(x)$ and $\mathrm{T}_{a_x}(u)$ is a characteristic function given by the Fourier transform of $\Pi(-x/a_x)$. The aperture MTF, or "del" MTF, describes how spatial frequencies are passed through the detector elements. When quanta are integrated in elements of width a_x, the aperture MTF is given by

$$\mathrm{MTF}_{a_x}(u) = \frac{|\mathrm{T}_{a_x}(u)|}{\mathrm{T}_{a_x}(0)} = \left|\mathrm{sinc}(\pi a_x u)\right|.\qquad(2.189)$$

As the widths of detector elements are decreased, the bandwidth of the aperture MTF is increased.

2.9.2 Digital MTF: presampling MTF and aliasing

The quantity $d(x)$ is the presampling detector signal as described in the previous section, and evaluation of $d(x)$ at the centers of each detector element gives the detector signal for each element. The process of evaluating a function is called sampling (Section 2.2.2). Evaluating $d(x)$ at positions $x = nx_0$ for all n can be represented as multiplication with the comb function $\sum \delta(x - nx_0)$ giving $d^\dagger(x)$, where

$$d^\dagger(x) = d(x) \sum_{n=-\infty}^{\infty} \delta(x - nx_0) = \sum_{n=-\infty}^{\infty} d_n \delta(x - nx_0), \qquad (2.190)$$

which consists of an infinite train of δ functions scaled by the detector values d_n. This process is illustrated in the two domains in Figure 2.29. Multiplication with $\sum_{n=-\infty}^{\infty} \delta(x - nx_0)$ in the spatial domain corresponds to convolution with $(1/x_0) \sum_{n=-\infty}^{\infty} \delta(u - 1/nx_0)$ in the spatial-frequency domain. Therefore, the Fourier transform of $d^\dagger(x)$ is given by

$$F\{d^\dagger(x)\} = D(u) * \frac{1}{x_0} \sum_{n=-\infty}^{\infty} \delta\left(u - \frac{1}{nx_0}\right), \qquad (2.191)$$

as illustrated in Figure 2.29 where $D(u)$ is the Fourier transform of $d(x)$. This illustration shows that sampling $d(x)$ at uniform spacings of x_0 corresponds to
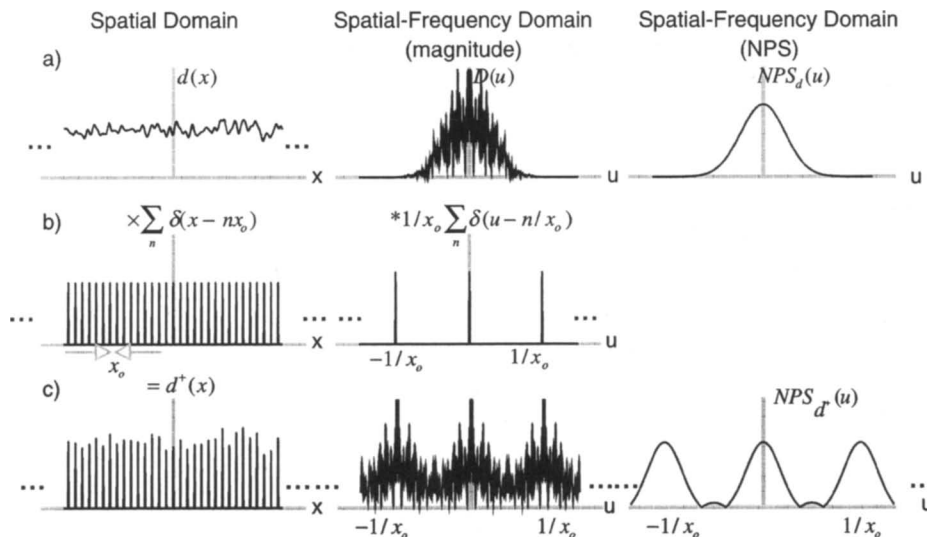

Figure 2.29: Sampling a function at uniform spacing x_0 results in spectral aliasing if the presampling signal $d(x)$ has frequency components above the sampling cut-off frequency $u_c = 1/2x_0$.

the production of aliases of $D(u)$ at spacings of $u = 1/x_0$. If the aliases overlap, aliasing occurs, resulting in a distortion of the image signal at frequencies below the sampling cut-off frequency, $u_c = 1/(2x_0)$. Excellent descriptions of sampling and aliasing in medical-imaging systems are given elsewhere by Barrett and Swindell [13], and Metz and Doi [12] among others.

In this section, the effect of the digital detector has been described as a two-step process: (1) integration of interacting input quanta in each element to produce a presampling detector signal; and, (2) evaluation (sampling) of the presampling detector signal to generate the individual detector-element values d_n. In the spatial-frequency domain, these two processes are described in terms of: (1) the presampling MTF, $\text{MTF}_{pre}(u)$; and, (2) aliasing as determined by the sample spacing x_0. The overall effect of the detector in the Fourier domain therefore is to attenuate spatial frequencies by the presampling MTF and to introduce aliasing if frequencies remain that are greater than the sampling cut-off frequency given by $u_c = 1/(2x_0)$. Both steps are required for the description of digital detectors. The presampling MTF can be measured on real systems using techniques such as the slanted-edge method [29, 51, 52]. Dobbins et al. [53] describe the effects of aliasing and Fourier-domain phase errors resulting from an inadequate sampling frequency that may be encountered with digital detectors.

Of particular importance is the case of ideal dels of width x_0 with no spaces between the active regions of each del, corresponding to a unity detector fill factor. The presampling MTF is given by $\text{MTF}_{pre}(u) = |\text{sinc}(\pi x/x_0)|$ which has the first zero at $u = 1/x_0$, twice the sampling cut-off frequency, and aliasing may be hard to avoid. If the detector fill factor is less than unity, the bandwidth of the presampling MTF is increased further, resulting in more aliasing. Aliasing can sometimes be reduced with the appropriate use of a spatial "anti-aliasing" filter of some sort, such as the scattering of light in the scintillating screen of indirect flat-panel detector.

2.9.3 Digital NPS: presampling NPS and noise aliasing

The NPS has been defined in Sections 2.5.5 and 2.5.6 for only WSS and WSCS random processes. However, a digital image consists of an array of discrete values, d_n, which represent neither a WSS nor a WSCS random process. This minor dilemma is avoided with the linear-systems approach by noting that d_n are samples of the detector presampling signal $d(x)$ where $d(x)$ describes a WSS random process, and the resulting sampled signal $d^\dagger(x)$, an array of δ functions scaled by the values d_n, represents a WSCS random process. The NPS of $d^\dagger(x)$ is therefore given by Eq. (2.110) as

$$\text{NPS}_{d^\dagger}(u) = \frac{1}{x_0^2}\,\text{NPS}_d(u) * \sum_{n=-\infty}^{\infty} \delta\left(u - \frac{n}{x_0}\right) \qquad (2.192)$$

$$= \frac{1}{x_0^2}\left[\text{NPS}_d(u) + \sum_{n=1}^{\infty}\text{NPS}_d\left(u \pm \frac{n}{x_0}\right)\right], \qquad (2.193)$$

as illustrated in Figure 2.30(c). It is clear from Eq. (2.193) that the NPS of $d^\dagger(x)$ consists of a fundamental presampling NPS, $\text{NPS}_d(u)$, plus aliases centered at the frequencies $u = n/x_0$, scaled by the factor $1/x_0^2$. If the aliases overlap, noise aliasing takes place, potentially increasing image noise at all frequencies below the sampling cut-off frequency.

The sampling theorem states that frequencies above the cut-off frequency $u_c = 1/(2x_0)$ cannot be represented with samples obtained with a uniform sampling frequency of $u_s = 1/x_0$. We therefore introduce $\text{NPS}_{\hat{d}}(u)$ which is truncated to this frequency range, and is the NPS of $\hat{d}(x)$. Truncation in the frequency domain corresponds to convolution with a sinc function in the spatial domain, and hence $\hat{d}(x)$ is given by

$$\hat{d}(x) = \sum_{n=-\infty}^{\infty} d_n \,\text{sinc}\left(\pi \frac{x - nx_0}{x_0}\right) \tag{2.194}$$

$$= d^\dagger(x) * \text{sinc}(\pi x_0 u), \tag{2.195}$$

which is an estimate of $d(x)$, equal to a "sinc" interpolation of the digital values d_n, as illustrated in Figure 2.30(e). The NPS of $\hat{d}(x)$ is $\text{NPS}_{\hat{d}}(u)$ given by

$$\text{NPS}_{\hat{d}}(u) = \text{NPS}_{d^\dagger}(u) x_0^2 \prod (x_0 u). \tag{2.196}$$

The functions $d(x)$ and $\hat{d}(x)$ are equal only if there is no aliasing of $d(x)$.

When the DFT is defined by Eq. (2.63), the NPS estimated from one-dimensional digital data can be written as

$$\text{NPS}_{dig}(u)\Big|_{u=\frac{m}{Nx_0}} = \frac{x_0}{N} \,\text{E}\left\{\left|\text{DFT}\{\Delta d_n\}\right|^2\right\}, \tag{2.197}$$

where $\Delta d_n = d_n - \text{E}\{d_n\}$ and is called here the *digital NPS*. It is defined only for the frequencies evaluated by the DFT, which are $u = m/Nx_0$ for $-N/2 \leqslant m \leqslant N/2 - 1$. At these frequencies it is also equal to $\text{NPS}_{\hat{d}}(u)$, and therefore $\text{NPS}_{dig}(u)$ is related to the presampling NPS, $\text{NPS}_d(u)$, by

$$\text{NPS}_{dig}(u) = \text{NPS}_{\hat{d}}(u) \tag{2.198}$$

$$= x_0^2 \text{NPS}_{d^\dagger}(u) \tag{2.199}$$

$$= \text{NPS}_d(u) + \sum_{n=1}^{\infty} \text{NPS}_d\left(u \pm \frac{n}{x_0}\right), \tag{2.200}$$

explicitly stating the undesirable effects of noise aliasing with the second term. It is satisfying to note that Eq. (2.197) can be viewed as a numerical estimate of the NPS of $d(x)$ given by Eq. (2.93). Equation (2.200) for the digital NPS was first described to the medical imaging community by Giger [54].
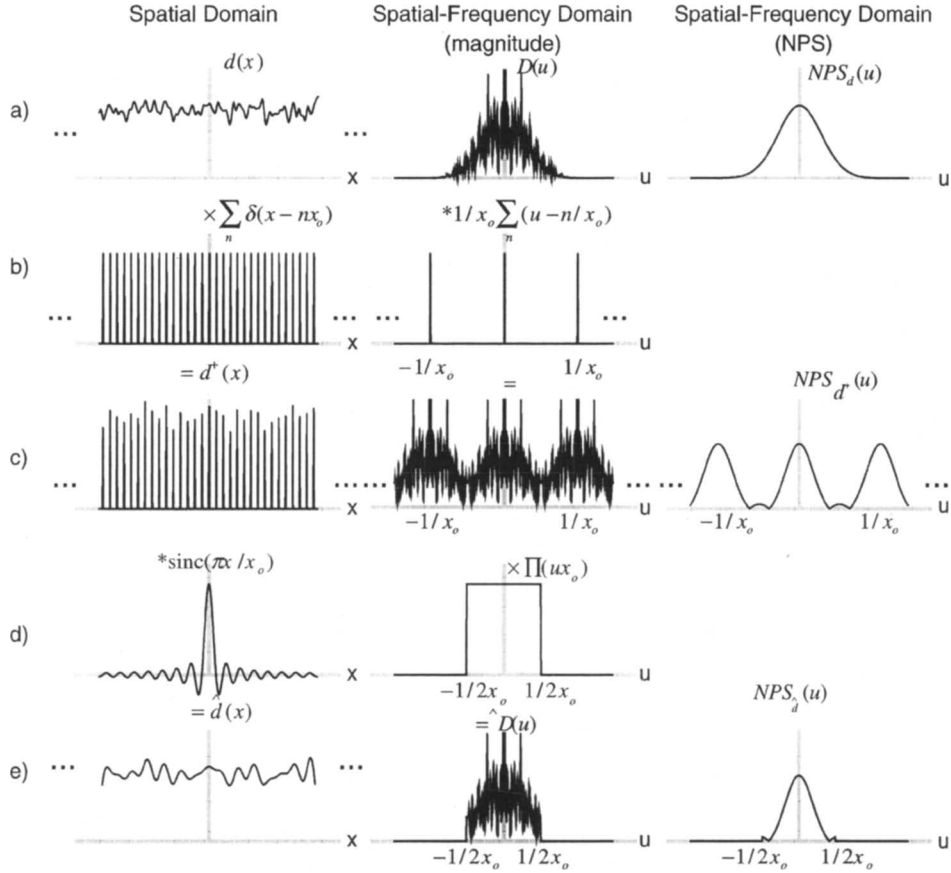
Figure 2.30: Schematic illustration describing the NPS of a digital image in terms of the Fourier transform. Left: spatial domain. Center: magnitude, spatial-frequency domain. Right: NPS.

2.9.3.1 Digital NPS in two dimensions

The digital NPS for a one-dimensional noise process is given by Eq. (2.197). However, digital images represent two-dimensional noise processes and hence it is necessary to make use of the two-dimensional digital NPS for image analyses which is given by

$$\text{NPS}_{dig}(u, v) = \frac{x_0 y_0}{N_x N_y} \, \text{E}\left\{\left|\text{DFT}^{2D}\{\Delta d_{n_x, n_y}\}\right|^2\right\}, \qquad (2.201)$$

for the frequencies evaluated by the two-dimensional DFT, DFT^{2D}, where x_0 and y_0 are the x and y spacings of the discrete values respectively. The one-dimensional NPS of the two-dimensional noise process represented by a digital image is given

by

$$\text{NPS}_{dig}(u) = \frac{x_0 y_0}{N_x N_y} \, \mathrm{E} \left\{ \left| \text{DFT}\left\{ \sum_{n_y=0}^{N_y-1} \Delta d_{n_x,n_y} \right\} \right|^2 \right\}. \tag{2.202}$$

Equation (2.202) should be considered a working definition of the digital NPS for systems analysis after ensuring that the DFT being used is consistent with Eq. (2.63). The expectation value of the squared DFT can be estimated by squaring and averaging the DFT of many digital noise images.

2.9.3.2　Digital-detector noise variance

The noise variance in $d(x)$ is conserved by the process of noise aliasing so that

$$\sigma_d^2 = \int_{-\infty}^{\infty} \text{NPS}_d(u) \, du \tag{2.203}$$

$$= x_0^2 \int_{-1/2x_0}^{1/2x_0} \text{NPS}_{d^\dagger}(u) \, du \tag{2.204}$$

$$= \int_{-1/2x_0}^{1/2x_0} \text{NPS}_d(u) + \sum_{n=1}^{\infty} \text{NPS}_d\left(u \pm \frac{n}{x_0}\right) du. \tag{2.205}$$

Noise aliasing cannot be undone once it has occurred. It can be prevented only by implementing a spatial anti-aliasing filter which would reduce the bandwidth of the presampling NPS, $\text{NPS}_d(u)$, such that negligible noise power exists at frequencies above the sampling cut-off frequency. The calculated pixel variance is given by

$$\sigma_d^2 = \frac{1}{N-1} \sum_{n=0}^{N-1} |\Delta d_n|^2. \tag{2.206}$$

2.9.4　Digital NEQ

The NEQ as given by Eq. (2.145) applies to digital systems although made more complicated by the potential presence of signal and noise aliasing. The numerator describes the system transfer of signals from the input to the output, and thus the MTF for digital systems is the presampling MTF which includes the aperture MTF. Noise in a digital image is given by Eq. (2.200) and so the digital NEQ is given by

$$\text{NEQ}_{dig}(\bar{q}, u) = \frac{\bar{q}^2 \left| \frac{\partial \bar{d}}{\partial \bar{q}} \right|^2 \text{MTF}_{pre}^2(u)}{\text{NPS}_{dig}(u)}, \tag{2.207}$$

for $u = m/Nx_0$ and $-N/2 \leqslant m \leqslant N/2 - 1$, where x_0 is the center-to-center spacing of detector elements. Thus, for linear digital systems, the NEQ can be calculated using

$$\mathrm{NEQ}_{dig}(\overline{q}, u) = \frac{\mathrm{MTF}^2_{pre}(u)}{\mathrm{NPS}_{dig}(u)/\overline{d}^2},$$ (2.208)

for $u = m/Nx_0$ and $-N/2 \leqslant m \leqslant N/2 - 1$ when using a DFT given by Eq. (2.63) and where $\mathrm{NPS}_{dig}(u)$ is given by Eq. (2.202). Interpretation of the digital NEQ is possibly easier when expressed in the form

$$\mathrm{NEQ}_{dig}(\overline{q}, u) = \frac{\overline{d}^2\mathrm{MTF}^2_{pre}(u)}{\left[\mathrm{NPS}_d(u) + \sum_{n=1}^{\infty}\mathrm{NPS}_d\left(u \pm \frac{n}{x_0}\right)\right]},$$ (2.209)

for $u = m/Nx_0$ and $-N/2 \leqslant m \leqslant N/2 - 1$. The NEQ is a measure of the noise-equivalent number of quanta, and is affected by noise aliasing. Signal aliasing adds an additional artifact that is not included in the NEQ. The digital NEQ is defined only for frequencies less than the sampling cut-off frequency, $u_c = 1/2x_0$.

2.9.5 Digital DQE

Similar to the digital NEQ, the digital DQE is defined here as

$$\mathrm{DQE}_{dig}(\overline{q}, u) = \frac{\mathrm{NEQ}_{dig}(\overline{q}, u)}{\overline{q}}$$ (2.210)

$$= \frac{\overline{d}^2\mathrm{MTF}^2_{pre}(u)}{\overline{q}\left[\mathrm{NPS}_d(u) + \sum_{n=1}^{\infty}\mathrm{NPS}_d\left(u \pm \frac{n}{x_0}\right)\right]},$$ (2.211)

for $u = m/Nx_0$ and $-N/2 \leqslant m \leqslant N/2 - 1$.

2.9.6 Signal aliasing

Signal aliasing can also be viewed as a form of image noise, but depends on specifics of particular images and is not WSS or WSCS. It is therefore not included in the calculations presented in this chapter. However, it is still important to remember that signal aliasing may result in additional artifacts and image degradation.

2.10 Analysis of a simple digital detector array

The DQE of a (hypothetical) simple digital detector is described here as an illustrative example of principles presented here. The detector is illustrated in Figure 2.31. It consists of a thin scintillating screen bonded to an optical detector array.
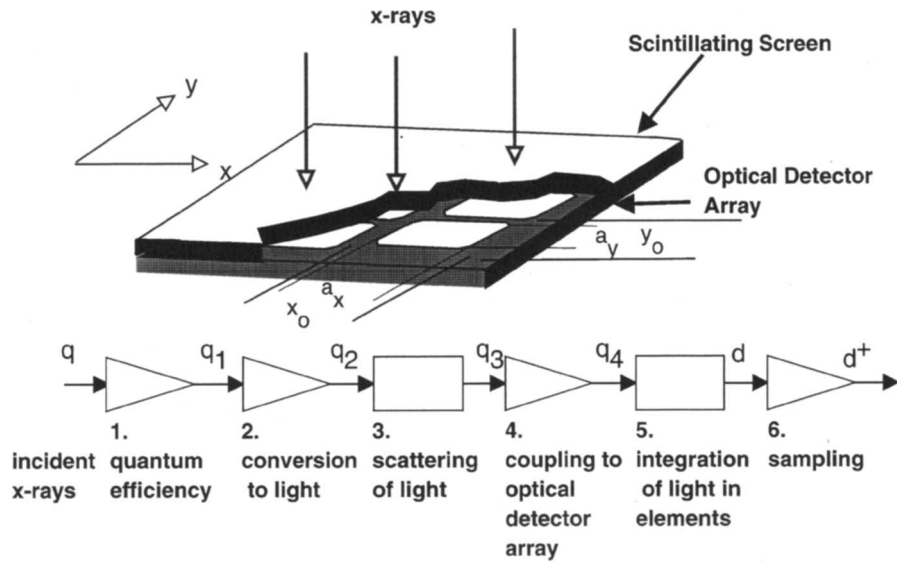
Figure 2.31: Schematic illustration of the hypothetical simple digital detector. The linear-systems model consists of 6 stages.

While this model is not intended to represent any particular imaging system, it is essentially a simple model of a hypothetical flat-panel thin-film-transistor (TFT) array detector, similar to any of several designs being developed elsewhere for radiographic and fluoroscopic applications [55, 56].

2.10.1 Cascaded model

The detector array is modeled as a cascade of six linear stages (Figure 2.31). The input is a uniform distribution of x-ray quanta represented as the quantum image $q_0(x, y)$ (Section 2.2.1.3) with an expected value of $\overline{q}_0$ quanta/mm^2. The NPS of this input quantum image is therefore $\mathrm{NPS}_0(k) = \overline{q}_0$ (see Section 2.6.2.3). Transfer of the expected value and NPS through stage 5 and 6 is illustrated in Figure 2.32.

2.10.1.1 Stage 1: selection of x-ray quanta that interact in screen

Selection of incident x-ray quanta that interact in the screen is represented as a quantum selection stage (Section 2.7.1.1), which is a special case of quantum amplification. If the quantum efficiency is α, $\widetilde{\alpha}$ is introduced as a random variable having the values 0 and 1 only with an expected value α. Therefore, using Eqs. (2.160) and (2.164), the distribution of interacting quanta can be represented as $q_1(r)$ having an expected value of $\overline{q}_1$ and NPS of $\mathrm{NPS}_1(k)$ where

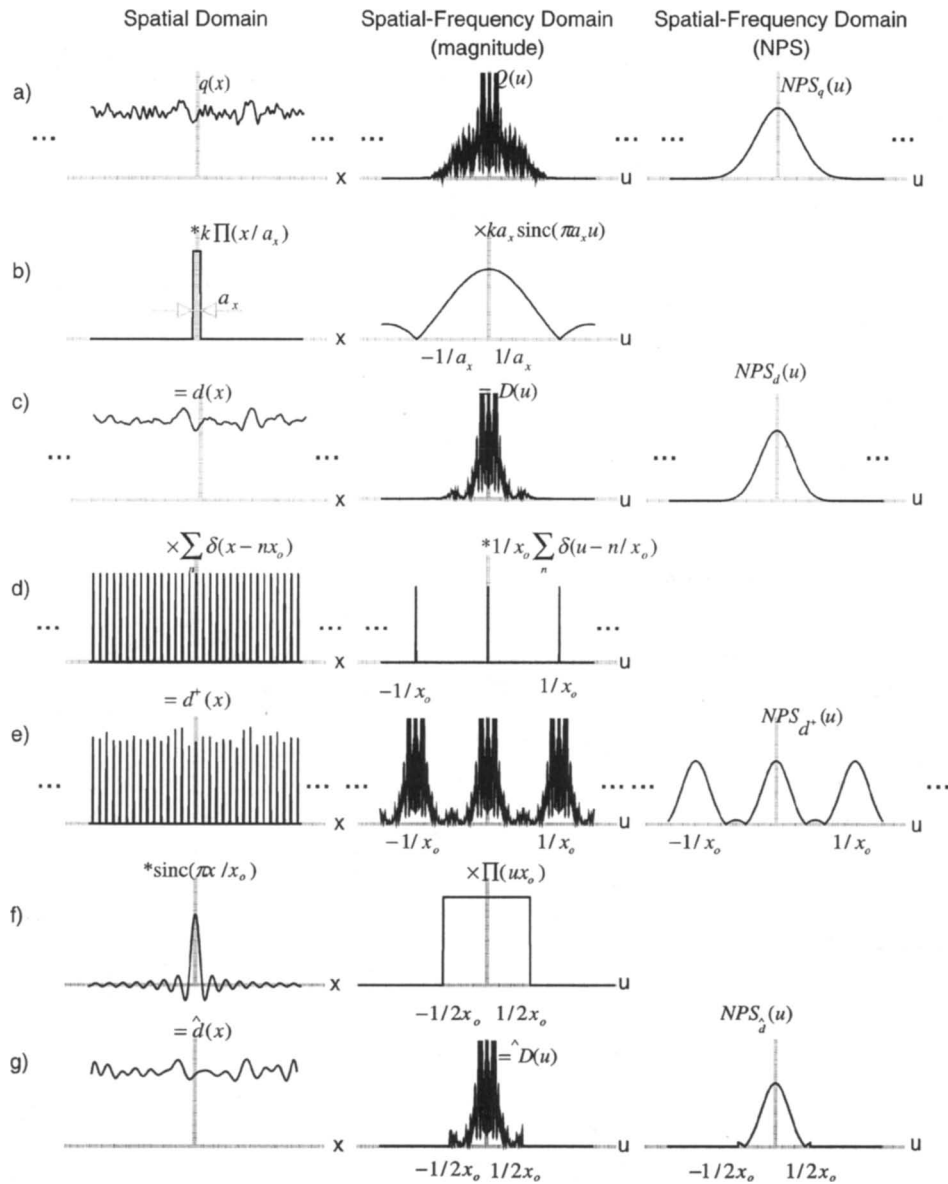$$q_1(r) = q_0(r)\widetilde{\alpha}, \tag{2.212}$$

Figure 2.32: Transfer of the expected number of image quanta and corresponding NPS at each stage of the cascaded model. Left: spatial domain. Center: spatial-frequency domain (magnitude). Right: NPS.

$$\overline{q}_1 = \alpha \overline{q}_0, \tag{2.213}$$

and

$$\mathrm{NPS}_1(k) = \alpha \overline{q}_0, \tag{2.214}$$

in units of mm^{-2}.

2.10.1.2 Stage 2: conversion to optical quanta in screen

It is assumed that each interacting quantum produces an average of $\overline{m}$ optical quanta per interaction with a variance σ_m^2. This variance accounts for all variations in the conversion gain, including Swank noise and a polychromatic x-ray beam. The conversion gain (Section 2.7.1) is therefore represented as the random variable $\widetilde{m}$ and the resulting distribution of optical quanta, expected value and NPS is obtained using Eqs. (2.160) and (2.161) giving

$$q_2(r) = q_0(r)\widetilde{m}\widetilde{\alpha}, \tag{2.215}$$

$$\overline{q}_2 = \alpha \overline{m}\,\overline{q}_0, \tag{2.216}$$

and

$$\mathrm{NPS}_2(k) = \alpha \overline{m}^2 \overline{q}_0 \left(1 + \frac{\varepsilon_m}{\overline{m}} \right) + \alpha \overline{m}\,\overline{q}_0, \tag{2.217}$$

in units of mm^{-2}.

2.10.1.3 Stage 3: scattering of optical quanta in screen

It is assumed that all light quanta scatter (Section 2.7.3) with the same point-spread function $\mathrm{psf}_s(x, y)$ normalized to unity area, neglecting variable interaction depths in the screen. The resulting quantum image, expected value and NPS are obtained using Eqs. (2.170) and (2.171) giving

$$q_3(r) = q_0(r)\widetilde{m}\widetilde{\alpha} *_s \mathrm{psf}_s(r), \tag{2.218}$$

$$\overline{q}_3 = \alpha \overline{m}\,\overline{q}_0, \tag{2.219}$$

and

$$\mathrm{NPS}_3(k) = \alpha \overline{m}^2 \overline{q}_0 \left(1 + \frac{\varepsilon_m}{\overline{m}} \right) |\mathrm{MTF}_s(k)|^2 + \alpha \overline{m}\,\overline{q}_0, \tag{2.220}$$

in units of mm^{-2} where $*_s$ represents the scattering process [42] and $\mathrm{MTF}_s(k)$ is the scatter MTF. The gain Poisson excess ε_m is related to the gain variance as given by Eq. (2.177).

2.10.1.4 Stage 4: selection of light quanta that interact

It is assumed that a fraction β of all light quanta will interact somewhere in the optical detector array. The factor β must include the coupling efficiency of light from the screen as well as the quantum efficiency of the detector array. It does not matter *where* the light quanta interact, and it does not matter if they interact in an active or inactive region. The factor β describes only the probability of interaction. The expected value and NPS of the distribution of interacting light quanta is therefore obtained using Eqs. (2.160) and (2.164), giving

$$q_4(\mathbf{r}) = q_0(\mathbf{r})\widetilde{m}\widetilde{\alpha} *_s \mathrm{psf}_s(\mathbf{r})\widetilde{\beta}, \tag{2.221}$$

$$\overline{q}_4 = \alpha\overline{m}\beta\overline{q}_0, \tag{2.222}$$

and

$$\mathrm{NPS}_4(\mathbf{k}) = \alpha\overline{m}^2\beta^2\overline{q}_0\left(1 + \frac{\varepsilon_m}{\overline{m}}\right)|\mathrm{MTF}_s(\mathbf{k})|^2 + \alpha\overline{m}\beta\overline{q}_0, \tag{2.223}$$

in units of mm^{-2}.

2.10.1.5 Stage 5: spatial integration of interacting light quanta in elements

The detector presampling signal is given by the integral of $q_4(\mathbf{r})$ over rectangles with width a_x and a_y corresponding to the width of active regions of the detector elements, corresponding to a deterministic blur stage (Section 2.7.2). If k is the scaling factor relating the number of interacting light quanta to the output signal, the detector presampling signal is given in Cartesian coordinates by

$$d(x, y) = k\left\{\left[q_0(x, y)\widetilde{m}\widetilde{\alpha}\right] *_s \mathrm{psf}_s(x, y)\widetilde{\beta} * \prod\left(\frac{x}{a_x}, \frac{y}{a_y}\right)\right\}, \tag{2.224}$$

where $*$ represents a two-dimensional convolution integral. The expected detector signal $\overline{d}$ is given by

$$\overline{d} = ka_x a_y \alpha\overline{m}\beta\overline{q}_0, \tag{2.225}$$

which is unitless, and the NPS by

$$\mathrm{NPS}_d(u, v) = k^2 a_x^2 a_y^2\left[\alpha\overline{m}^2\beta^2\overline{q}_0\left(1 + \frac{\varepsilon_m}{\overline{m}}\right)|\mathrm{MTF}_s(u, v)|^2 + \alpha\overline{m}\beta\overline{q}_0\right]$$
$$\times |\mathrm{sinc}(\pi a_x u)|^2|\mathrm{sinc}(\pi a_y v)|^2, \tag{2.226}$$

in units of mm^2. Note that it is at this stage, after integration of quanta in detector elements, one must start representing the image as an analog image rather than as a quantum image. As a consequence, units of the NPS are mm^2 rather than mm^{-2}.

2.10.1.6 Stage 6: output from discrete detector elements

The process of obtaining the discrete output signals from each detector element is represented as a sampling process. If each detector element has a center-to-center spacing of x_0 and y_0 in the x and y directions respectively, the sampled detector signal $d^\dagger(x, y)$ is given by

$$d^\dagger(x, y) = k\left\{ \left[q_0(x, y)\widetilde{m}\widetilde{\alpha} \right] *_s \mathrm{psf}_s(x, y)\widetilde{\beta} * \prod\left(\frac{x}{a_x}, \frac{y}{a_y} \right) \right\}$$

$$\times \sum_{n_x=-\infty}^{\infty} \sum_{n_y=-\infty}^{\infty} \delta(x - n_x x_0, y - n_y y_0) \qquad (2.227)$$

The expected value is given by

$$\mathrm{E}\{d^\dagger(x, y)\} = k a_x a_y \alpha \overline{m} \beta \overline{q}_0 \sum_{n_x=-\infty}^{\infty} \sum_{n_y=-\infty}^{\infty} \delta(x - n_x x_0, y - n_y y_0), \qquad (2.228)$$

consisting of two-dimensional δ functions scaled by the digital values d_{n_x,n_y} where the expected value of d_{n_x,n_y} is

$$\mathrm{E}\{d_{n_x,n_y}\} = k a_x a_y \alpha \overline{m} \beta \overline{q}_0. \qquad (2.229)$$

The NPS of $d^\dagger(x, y)$, obtained using Eq. (2.193) and generalized to two dimensions, is given by

$$\mathrm{NPS}_d^\dagger(u, v) = \frac{1}{x_0^2 y_0^2}\left[\mathrm{NPS}_d(u, v) + \sum_{n_x=1}^{\infty} \sum_{n_y=1}^{\infty} \mathrm{NPS}_d\left(u \pm \frac{n_x}{x_0}, v \pm \frac{n_y}{y_0} \right) \right]. \qquad (2.230)$$

Combining this result with Eqs. (2.199) and (2.226) gives the two-dimensional digital NPS as

$$\mathrm{NPS}_{dig}(u, v) = \mathrm{NPS}_d(u, v) + \sum_{n_x=1}^{\infty} \sum_{n_y=1}^{\infty} \mathrm{NPS}_d\left(u \pm \frac{n_x}{x_0}, v \pm \frac{n_y}{y_0} \right), \qquad (2.231)$$

for frequencies below the sampling cut-off frequencies of $u_c = 1/2x_0$ and $v_c = 1/2y_0$. The digital NPS has units of mm^2.

The one-dimensional NPS of this two-dimensional noise process is obtained by evaluating Eq. (2.231) along the appropriate axis. The NPS in the x direction is obtained by setting $v = 0$ and substituting d_n for d_{n_x}, giving

$$\mathrm{NPS}_{dig}(u) = \mathrm{NPS}_d(u) + \sum_{n=1}^{\infty} \mathrm{NPS}_d\left(u \pm \frac{n}{x_0}\right), \qquad (2.232)$$

which also has units mm^2 and where $\mathrm{NPS}_d(u)$ is the presampling NPS of $d(x)$.

2.10.2 Detector DQE

The DQE of this hypothetical detector is evaluated in the x direction only to simplify the mathematical expressions by setting $v = 0$. The DQE is given by Eq. (2.211) where the presampling MTF is given by

$$\mathrm{MTF}_{pre}(u) = \mathrm{MTF}_s(u)\left|\mathrm{sinc}(\pi a_x u)\right|, \qquad (2.233)$$

and the presampling NPS by Eq. (2.226). In the absence of additive noise, these results can be combined, giving

$$\mathrm{DQE}(u) = \frac{\alpha \mathrm{MTF}_s^2(u)\mathrm{sinc}^2(\pi a_x u)}{F(u) + \sum_{n=1}^{\infty} F\left(u \pm \frac{n}{x_0}\right)}, \qquad (2.234)$$

where

$$F(u) = \left[\left(1 + \frac{\varepsilon_m}{m}\right)\mathrm{MTF}_s^2(u) + \frac{1}{m\beta}\right]\mathrm{sinc}^2(\pi a_x u). \qquad (2.235)$$

This result offers little insight into important physical processes without making some simplifications. For instance, if $\overline{m}\beta > 100$ as required by the QAD condition (Section 2.8.3) to prevent secondary quantum sinks, then $(\overline{m}\beta)^{-1} \ll |\mathrm{MTF}_{pre}(u)|^2$ for all frequencies passed by $\mathrm{MTF}_{pre}(u)$ with any significance. If it is further assumed that the conversion gain from X rays to light is approximately Poisson so that $|\varepsilon_m/\overline{m}| \ll 1$ (a good assumption for many scintillating screens including CsI), the DQE simplifies to

$$\mathrm{DQE}(u)$$

$$\approx \frac{\alpha \mathrm{MTF}_s^2(u)\mathrm{sinc}^2(\pi a_x u)}{\mathrm{MTF}_s^2(u)\mathrm{sinc}^2(\pi a_x u) + \sum_{n=1}^{\infty}\mathrm{MTF}_s^2\left(u \pm \frac{n}{x_0}\right)\mathrm{sinc}^2\left(\pi a_x\left[u \pm \frac{n}{x_0}\right]\right)} \qquad (2.236)$$

$$= \frac{\alpha \mathrm{MTF}_{pre}^2(u)}{\mathrm{MTF}_{pre}^2(u) + \sum_{n=1}^{\infty}\mathrm{MTF}_{pre}^2\left(u \pm \frac{n}{x_0}\right)}. \qquad (2.237)$$

2.10.3 Noise aliasing, detector fill factor and variance

The effect of noise aliasing on the DQE is given by the second term in the denominator of Eq. (2.237). Noise aliasing can only be avoided if $\text{MTF}_{pre}^2(u) \ll 1$ for all frequencies above the sampling cut-off frequency $|u| \geqslant u_c$ where $u_c = 1/2x_0$ (Figure 2.32). Two limiting cases are considered as described below.

2.10.3.1 Low-resolution scintillator (correlated quantum noise on detector array)

A "low"-resolution scintillator implies that the system MTF in the x direction is limited by the screen and not by the detector element size a_x. The screen causes the quantum noise in the optical image incident on the optical detector array to be correlated, which reduces the noise bandwidth. Thus, $\text{sinc}^2(\pi a_x u)$ is approximately constant for all frequencies of significance passed by $\text{MTF}_s^2(u)$ and the DQE simplifies to

$$\text{DQE}(u) \approx \frac{\alpha \text{MTF}_s^2(u)}{\text{MTF}_s^2(u) + \sum_{n=1}^{\infty} \text{MTF}_s^2\left(u \pm \frac{n}{x_0}\right)}. \tag{2.238}$$

If the detector elements are sufficiently small and close together that aliasing can be neglected, that is, $\text{MTF}_s^2(u)|_{u=u_c} \ll 1$ for $u_c = 1/2x_0$, the DQE reduces to

$$\text{DQE}(u) \approx \frac{\alpha \text{MTF}_s^2(u)}{\text{MTF}_s^2(u)} = \alpha. \tag{2.239}$$

Thus, for this special case of a quantum-noise-limited detector with sufficiently small detector elements and no secondary quantum sink, both image signal and noise are proportional to the MTF in the same way and the DQE is therefore flat with frequencies and determined entirely by the quantum efficiency of the screen α, not by the optical digital detector array. In particular, the DQE is not degraded by the detector fill factor $\gamma_x \gamma_y$, defined by $\gamma_x = a_x/x_0$ and $\gamma_y = a_y/y_0$, having a value less than unity. This result is only valid as long as additive detector noise can be neglected. For instance, if the detector fill factor is decreased, the signal decreases and there may be a point at which detector noise can no longer be neglected and where this result is not valid. The DQE of a two-dimensional detector array is given by the same result.

Image noise measured as the variance σ_d^2 in detector element values d_n is calculated by

$$\sigma_d^2 = \frac{1}{N-1} \sum_{n=0}^{N-1} [d_n - \overline{d}]^2. \tag{2.240}$$

The variance is also equal to the presampling NPS integrated over all frequencies (in two dimensions), given by

$$\sigma_d^2 = \int_{-\infty}^{\infty} \int_{-\infty}^{\infty} \text{NPS}_d(u, v) \, du \, dv \tag{2.241}$$

$$= \int_{-\infty}^{\infty} \int_{-\infty}^{\infty} k^2 a_x^2 a_y^2 \left[\alpha \overline{m}^2 \beta^2 \overline{q}_0 \left(1 + \frac{\varepsilon_m}{\overline{m}} \right) \text{MTF}_s^2(u, v) + \alpha \overline{m} \beta \overline{q}_0 \right]$$

$$\times \text{sinc}^2(\pi a_x u) \text{sinc}^2(\pi a_y v) \, du \, dv, \tag{2.242}$$

which simplifies to

$$\sigma_d^2 \approx k^2 a_x^2 a_y^2 \alpha \overline{m}^2 \beta^2 \overline{q}_0 \int_{-\infty}^{\infty} \int_{-\infty}^{\infty} \text{MTF}_s^2(u, v) \, du \, dv. \tag{2.243}$$

Thus, for the low-resolution scintillator detector, noise variance is proportional to the integral of the squared MTF. If the spatial resolution of the scintillator is degraded, the width of the MTF is reduced and detector variance decreases. This means that for a specified detector-element size, less detector noise will be obtained if a lower-resolution scintillator is used and a compromise must be found between noise and resolution.

2.10.3.2 High-resolution scintillator (uncorrelated quantum noise on detector array)

A "high"-resolution scintillator implies that the system MTF in the x direction is limited by the detector-array aperture function rather than by the scintillator. This corresponds to system designs using very-high-resolution scintillators, and also to amorphous selenium "direct-detection" flat-panel detectors. Therefore, $\text{MTF}_s^2(u)$ is approximately constant over frequencies passed by $\text{sinc}^2(\pi a_x u)$ and the DQE simplifies to

$$\text{DQE}(u) \approx \frac{\alpha \text{sinc}^2(\pi a_x u)}{\text{sinc}^2(\pi a_x u) + \sum_{n=1}^{\infty} \text{sinc}^2 \left(\pi a_x \left[u \pm \frac{n}{x_0} \right] \right)}. \tag{2.244}$$

Zhao et al. [57] have shown that the sum of $\text{sinc}^2(\pi a_x u)$ and its aliases at harmonics of $u = 1/x_0$ is always equal to a constant given by

$$\text{sinc}^2(\pi a_x u) + \sum_{n=1}^{\infty} \text{sinc}^2 \left(\pi a_x \left[u \pm \frac{n}{x_0} \right] \right) = \frac{x_0}{a_x} = \frac{1}{\gamma_x}, \tag{2.245}$$
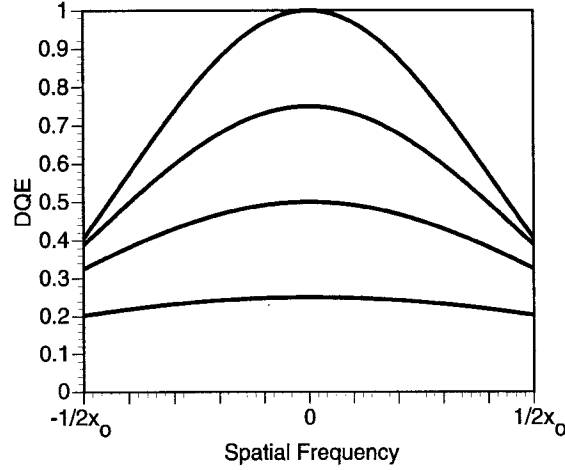
Figure 2.33: Illustration of the DQE for a two-dimensional detector with a high-resolution converter and fill-factor values $\gamma = \gamma_x \gamma_y$ (for $\gamma_x = \gamma_y$) equal to 1.0, 0.75, 0.50, and 0.25. The scintillator quantum efficiency, α, is assumed to be unity.

where $\gamma_x = a_x/x_0$ is the detector fill factor in the x direction. The DQE therefore reduces to

$$\mathrm{DQE}(u) \approx \alpha \, \frac{a_x}{x_0} \, \mathrm{sinc}^2(\pi a_x u) = \alpha \gamma_x \mathrm{sinc}^2(\pi a_x u), \qquad (2.246)$$

for a one-dimensional detector and to

$$\mathrm{DQE}(u, v) \approx \alpha \gamma_x \gamma_y \mathrm{sinc}^2(\pi a_x u) \mathrm{sinc}^2(\pi a_y v), \qquad (2.247)$$

for a two-dimensional detector. The one-dimensional DQE of this two-dimensional detector, evaluated along the $v = 0$ axis of the two-dimensional detector, is therefore given by

$$\mathrm{DQE}(u) \approx \alpha \gamma_x \gamma_y \mathrm{sinc}^2(\pi a_x u). \qquad (2.248)$$

Thus, for this special case of a quantum-noise-limited detector with a very-high-resolution converter, the DQE is proportional to the converter quantum efficiency α, and the detector fill factor $\gamma_x \gamma_y$, and always has a shape given by $\mathrm{sinc}^2(\pi a_x u)$, which is dependent on the x-direction fill factor. Figure 2.33 illustrates the DQE for a two-dimensional detector with a high-resolution scintillator for various fill factor values $\gamma = \gamma_x \gamma_y$ assuming $\gamma_x = \gamma_y$ based on Eq. (2.248). As the fill factor decreases, higher frequencies are passed by the detector-element apertures and noise aliasing increases. This is directly responsible for the decreasing DQE.

The detector variance is given by

$$\sigma_d^2 = \int_{-\infty}^{\infty} \int_{-\infty}^{\infty} \mathrm{NPS}_d(u, v) \, du \, dv \qquad (2.249)$$

$$\approx k^2 a_x^2 a_y^2 \alpha \overline{m}^2 \beta^2 \overline{q}_0 \int_{-\infty}^{\infty} \int_{-\infty}^{\infty} \text{sinc}^2(\pi a_x u) \text{sinc}^2(\pi a_y v) \, du \, dv \quad (2.250)$$

$$= k^2 a_x a_y \alpha \overline{m}^2 \beta^2 \overline{q}_0. \quad (2.251)$$

Thus, with the inclusion of noise aliasing, the noise variance predicted with this Fourier-based approach is equal to the variance that would be expected for a simple photon-counting detector of size $a_x \times a_y$.

It should also be noted that for this high-resolution scintillator (uncorrelated quantum noise incident on the detector array), the variance is related to the zero-frequency value of the NPS according to

$$\text{NPS}_d(0, 0) \approx a_x a_y \sigma_d^2, \quad (2.252)$$

consistent with Eq. (2.133).

2.11 Summary

In this chapter, principles of linear-systems theory have been summarized, including the point-spread function (PSF), line-spread function (LSF), modulation-transfer function (MTF), and other simple metrics of system performance. It has been shown how images may be classified as either quantum images (distributions of quanta), analog images, or digital images. Particular attention has been paid to the issue of units for each, and an introduction given to the principles of distribution theory and generalized functions that are essential for the description of quantum images.

These simple linear-systems metrics can be used to describe the *expected*, or *noise-free*, performance of an imaging system. However, they do not describe the transfer of image noise. The stochastic-theory relationships necessary to describe noise transfer are a very recent addition to the linear-systems approach, developed primarily by Shaw, Rabbani, Van Metter, and co-workers. In addition, the introduction of a photon-scatter operator to the linear-systems repertoire has allowed this approach to be extended to include the description of quantum-based *stochastic* systems, a necessary step for the description of medical-imaging systems. As a result, the extended linear-systems approach forms the basis from which comprehensive theoretical models of noise transfer through realistic imaging systems can be developed, and the connection is made to more complex metrics of system performance including the noise-power spectrum (NPS) and noise-equivalent number of quanta (NEQ).

It has also been shown how the linear-systems approach is used to develop cascaded-systems models that can be used to *predict*, based on theoretical design considerations, metrics of system performance including the spatial-frequency-dependent detective quantum efficiency (DQE). Complex imaging systems are represented as serial cascades of multiple "elementary" processes. This approach has been very successful for the theoretical analysis of many systems, and gives a physical interpretation to the idea of a spatial-frequency-dependent quantum sink. These

quantum sinks are responsible for the frequency dependence of the DQE except where limited by detector-noise sources. The cascaded approach provides a physically intuitive model that can be very helpful for understanding limitations of system performance and particular system designs, a necessary step for understanding and optimizing system performance in the design of new imaging systems.

Digital imaging systems add additional complexity to a systems analysis, requiring a description of noise aliasing. This has been accomplished using the theories of wide-sense cyclostationary (WSCS) random processes. While the description of WSCS processes has an established basis in communications theory, this author is unaware of their prior use in linear-systems theory or for the analysis or description of medical-imaging systems.

An illustrative example is given of the analysis of a hypothetical digital detector. The detector is essentially a simple model of a flat-panel active matrix detector similar to any of several designs currently under investigation and commercial production. The analysis shows how the DQE can be predicted from simple design parameters, and includes the effects of detector fill factor and noise aliasing on the DQE.

Acknowledgements

References

[1] Rose A. "A Unified Approach to the Performance of Photographic Film, Television Pick-Up Tubes, and the Human Eye." J Soc Motion Pict Telev Eng 47:273–294, 1946.

[2] Rose A. "Sensitivity Performance of the Human Eye on an Absolute Scale." J Opt Soc Am 38:196–208, 1948.

[3] Rose A. "Television Pickup Tubes and the Problem of Vision." In Marston (Ed.) *Advances in Electronics and Electron Physics*. New York: Academic Press, 1948, pp. 131–166.

[4] Rose A. "Quantum and Noise Limitations of the Visual Process." J Opt Soc Am 43:715–716, 1953.

[5] Dainty JC, Shaw R. *Image Science*. New York: Academic Press, 1974.

[6] Cunningham IA, Shaw R. "Signal-to-Noise Optimization of Medical Imaging Systems." J Opt Soc Am A16:621–632, 1999.

[7] Rossmann K. "Measurement of the Modulation Transfer Function of Radiographic Systems Containing Fluoroscent Screens." Phys Med Biol 9:551–557, 1964.

[8] Rossmann K. "The Spatial Frequency Spectrum: A Means for Studying the Quality of Radiographic Imaging Systems." Radiology 90:1–13, 1968.

[9] Gaskill JD. *Linear Systems, Fourier Transforms, and Optics*. New York: John Wiley & Sons, 1978.

[10] Papoulis A. *Systems and Transforms with Applications in Optics*. New York: McGraw-Hill, 1968.

[11] Doi K, Rossmann K, Haus AG. "Image Quality and Patient Exposure in Diagnostic Radiology." Photographic Science and Engineering 21:269–277, 1977.

[12] Metz CE, Doi K. "Transfer Function Analysis of Radiographic Imaging Systems." Phys Med Biol 24:1079–1106, 1979.

[13] Barrett HH, Swindell W. *Radiological Imaging—The Theory of Image Formation, Detection, and Processing*. New York: Academic Press, 1981.

[14] Bracewell RN. *The Fourier Transform and its Applications*, 2 Edition. New York: McGraw-Hill Book Company, 1978.

[15] Brigham EO. *The Fast Fourier Transform*. Englewood Cliffs, NJ: Prentice-Hall, 1974.

[16] Bendat JS, Piersol AG. *Random Data—Analysis and Measurement Procedures*, 2 Edition. New York: John Wiley & Sons, 1986.

[17] Papoulis A. *Probability, Random Variables, and Stochastic Processes*, 3 Edition. New York: McGraw Hill, 1991.

[18] Blackman RB, Tukey JW. *The Measurement of Power Spectra*. New York: Dover Publications, Inc, 1958.

[19] Shaw R, Van Metter RL. "An Analysis of the Fundamental Limitations of Screen-Film Systems for X-Ray Detection I. General Theory." In Schneider RH, Dwyer SJ (Eds.) *Application of Optical Instrumentation in Medicine XII*. Proc SPIE 454, 1984, pp. 128–132.

[20] Shaw R, Van Metter RL. "An Analysis of the Fundamental Limitations of Screen-Film Systems for X-Ray Detection II. Model Calculations." In Schneider RH, Dwyer SJ (Eds.) *Application of Optical Instrumentation in Medicine XII*. Proc SPIE 454, 1984, pp. 133–141.

[21] Van Metter RL. "Describing the Signal-Transfer Characteristics of Asymmetrical Radiographic Screen-Film Systems." Med Phys 19:53–58, 1992.

[22] Peters TM, Williams JC. *The Fourier Transform in Biomedical Engineering*. Boston: Birkhauser, 1998.

[23] Gardner NA, Franks LE. "Characteristics of Cyclostationary Random Signal Processes." IEEE Transactions in Information Theory IT-21: 1975.

[24] Fellgett PB. "On the Ultimate Sensitivity and Practical Performance of Radiation Detectors." J Opt Soc Am 39:970, 1949.

[25] Zwieg HJ. "Performance Criteria for Photo-Detectors—Concepts in Evolution." Photo Sc Eng 8:305–311, 1964.

[26] Jones RC. "A New Classification System for Radiation Detectors." J Opt Soc Am 39:327, 1949.

[27] Burgess AE. "The Rose Model, Revisited." J Opt Soc Am A16:633–646, 1999.

[28] "Medical Imaging—The Assessment of Image Quality." ICRU Report 54, 1995.

[29] Dobbins JT, Ergun DL, Rutz L, Hinshaw DA, Blume H, Clark DC. "DQE(f) of Four Generations of Computed Radiography Acquisition Devices." Med Phys 22:1581–1593, 1995.

[30] Shaw R. "The Equivalent Quantum Efficiency of the Photographic Process." J Photogr Sc 11:199–204, 1963.

[31] Wagner RF, Brown DG. "Unified SNR Analysis of Medical Imaging Systems." Phys Med Biol 30:489–518, 1985.

[32] Wagner RF. "Toward a Unified View of Radiological Imaging Systems. Part II: Noise Images." Med Phys 4:279–296, 1977.

[33] Wagner RF, Brown DG, Pastel MS. "Application of Information Theory to the Assessment of Computed Tomography." Med Phys 6:83–94, 1979.

[34] Sandrik JM, Wagner RF. "Absolute Measures of Physical Image Quality: Measurement and Application to Radiographic Magnification." Med Phys 9:540–549, 1982.

[35] Shaw R. "Some Fundamental Properties of Xeroradiographic Images." In Gray JE, Hendee WR (Eds.) *Application of Optical Instrumentation in Medicine IV*. Proc SPIE 70, 1975, pp. 359–363.

[36] Wagner RF, Muntz EP. "Detective Quantum Efficiency (DQE) Analysis of Electrostatic Imaging and Screen-Film Imaging in Mammography." In Gray JE (Ed.) *Application of Optical Instrumentation in Medicine VII*. Proc SPIE 173, 1979, pp. 162–165.

[37] Johns HE, Cunningham JR. *The Physics of Radiology*. Springfield IL: Charles C Thomas, 1983.

[38] Tucker DM, Barnes GT, Chakraborty DP. "Semiempirical Model for Generating Tungsten Target X-Ray Spectra." Med Phys 18:211–218, 1991.

[39] Rabbani M, Shaw R, Van Metter RL. "Detective Quantum Efficiency of Imaging Systems with Amplifying and Scattering Mechanisms." J Opt Soc Am A4:895–901, 1987.

[40] Metz CE, Vyborny CJ. "Wiener Spectral Effects of Spatial Correlation Between the Sites of Characteristic X-Ray Emission and Reabsorption in Radiographic Screen-Film Systems." Phys Med Biol 28:547–564, 1983.

[41] Barrett HH, Wagner RF, Myers KJ. "Correlated Point Processes in Radiological Imaging." In Van Metter RL, Beutel J (Eds.) *Medical Imaging 1997: Physics of Medical Imaging*. Proc SPIE 3032, 1997, pp. 110–125.

[42] Cunningham IA, Westmore MS, Fenster A. "Unification of Image Blur and Noise in Linear-Systems Transfer Theory Using a Quantum Scattering Operator." Med Phys 27:(accepted) 2000.

[43] Shockley W, Pierce JR. "A Theory of Noise for Electron Multipliers." Proc Inst Radio Eng 26:321–332, 1938.

[44] Ter-Pogossian MM. *The Physical Aspects of Diagnostic Radiology*. New York: Harper & Row, 1967.

[45] Mistretta CA. "X-Ray Image Intensifiers." In Haus AG (Ed.) AAPM No 3, *The Physics of Medical Imaging: Recording System Measurements and Techniques*. New York: American Institute of Physics, 1979, pp. 182–205.

[46] Macovski A. *Medical Imaging Systems*. Englewood Cliffs, NJ: Prentice-Hall, Inc., 1983.

[47] Roehrig H, Nudelman S, Fu TY. "Electro-Optical Devices for Use in Photoelectronic-Digital Radiology." In Fullerton GD, Hendee WR, Lasher JC, Properzio WS, Riederer SJ (Eds.) AAPM No 11, *Electronic Imaging in Medicine*. New York: American Institute of Physics, 1984, pp. 82–129.

[48] Roehrig H, Fu TY. "Physical Properties of Photoelectronic Imaging Devices and Systems." In Doi K, Lanzl L, Lin PJP (Eds.) AAPM No 12, *Recent Developments in Digital Imaging*. New York: American Institute of Physics, 1985, pp. 82–140.

[49] Cunningham IA, Westmore MS, Fenster A. "A Spatial-Frequency Dependent Quantum Accounting Diagram and Detective Quantum Efficiency Model of Signal and Noise Propagation in Cascaded Imaging Systems." Med Phys 21:417–427, 1994.

[50] Cunningham IA, Westmore MS, Fenster A. "Visual Impact of the Non-Zero Spatial Frequency Quantum Sink." In Shaw R (Ed.) *Medical Imaging 1994: Physics of Medical Imaging*. Proc SPIE 2163, 1994, pp. 274–283.

[51] Fujita H, Doi K, Giger ML. "Investigation of Basic Imaging Properties in Digital Radiography. 6. MTFs of II-TV Digital Imaging Systems." Med Phys 12:713–720, 1985.

[52] Holdsworth DW, Gerson RK, Fenster A. "A Time-Delay Integration Charge-Coupled Device Camera for Slot-Scanned Digital Radiography." Med Phys 17:876–886, 1990.

[53] Dobbins JT. "Effects of Undersampling on the Proper Interpretation of Modulation Transfer Function, Noise Power Spectra, and Noise Equivalent Quanta of Digital Imaging Systems." Med Phys 22:171–181, 1995.

[54] Giger ML, Doi K, Metz CE. "Investigation of Basic Imaging Properties in Digital Radiography. 2. Noise Wiener Spectrum." Med Phys 11:797–805, 1984.

[55] Antonuk LE, El-Mohri Y, Siewerdsen JH, Yorkston J, Huang W, Scarpine VE, Street RA. "Empirical Investigation of the Signal Performance of a High-Resolution, Indirect Detection, Active Matrix Flat-Panel Imager (AMFPI) for Fluoroscopic and Radiographic Operation." Med Phys 24:51–70, 1997.

[56] Siewerdsen JH, Antonuk LE, El-Mohri Y, Yorkston J, Huang W, Boudry JM, Cunningham IA. "Empirical and Theoretical Investigation of the Noise Performance of Indirect Detection, Active Matrix Flat-Panel Imagers (AMFPIs) for Diagnostic Radiology." Med Phys 24:71–89, 1997.

[57] Zhao W, Ji WG, Rowlands JA. "X-Ray Imaging Using Active Matrix Readout of Amorphous Selenium: Analysis of Detective Quantum Efficiency." Med Phys 1997.